Cellular/Molecular

Chronic Desipramine Reverses Deficits in Cell Activity, Norepinephrine Innervation, and Anxiety–Depression Phenotypes in Fluoxetine-Resistant cF1ko Mice

Faranak Vahid-Ansari, Amin Zahrai, <img>Mireille Daigle, and <img>Paul R. Albert

Ottawa Hospital Research Institute (Neuroscience), University of Ottawa, Ottawa, Ontario K1H-8M5, Canada

Selective serotonin (5-HT) reuptake inhibitors are only 30% effective for remission in subjects with major depression, and the best treatments for SSRI-resistant patients remain unclear. To model SSRI resistance, we used cF1ko mice with conditional deletion of the repressor Freud-1/CC2D1A in adult 5-HT neurons. Within weeks, this deletion leads to overexpression of 5-HT1A autoreceptors, reduced serotonergic activity, and fluoxetine-resistant anxiety–depression phenotype. We hypothesized that desipramine (DES), which targets norepinephrine (NE), may be effective in cF1ko mice. The actions of chronic DES treatment on behavior, chronic cellular activation, and NE projections were examined in both sexes of cF1ko and WT mice. In contrast to fluoxetine, chronic DES reversed the behavioral phenotypes in cF1ko mice, while in WT littermates DES slightly increased anxiety and depression-like behaviors. Deficits in FosB+ cell counts were seen in the entorhinal cortex, hippocampal CA2/3 layer, and BLA of cF1ko mice and were reversed by chronic DES treatment, especially in GABAergic neurons. In cF1ko mice, widespread reductions were seen in NE axons, varicosities, and especially 30–60% reductions in NE synaptic and triadic contacts, particularly to inhibitory gephyrin-positive sites. DES treatment also reversed these reductions in NE innervation. These results indicate the dynamic plasticity of the adult noradrenergic system within weeks of altering serotonergic function that can be normalized by DES treatment. Accompanying these changes, DES but not fluoxetine reversed the behavioral alterations in cF1ko mice, suggesting a key role for noradrenergic plasticity in antidepressant response in this model of reduced serotonin activity.

Key words: antidepressant; GABA; neuroplasticity; norepinephrine; synapses

---

Significance Statement

Reduced activity of the serotonin system is implicated in major depression. We have modeled this using cF1ko mice that overexpress the 5-HT1A receptor on serotonin neurons to inhibit them. These mice show depression-like behavior and do not respond to serotonin reuptake inhibitor fluoxetine, so we hypothesized that they would respond to desipramine (DES), which targets norepinephrine (NE) reuptake. DES not only reversed the behavioral phenotype but also restored NE innervation and cellular activity that were reduced in these mice. We conclude that DES induces a novel mechanism of region-specific noradrenergic reinnervation to restore NE activity and mediate behavioral recovery in cF1ko mice. These studies suggest that in this depression model with reduced serotonergic activity, antidepressant-induced neuroplasticity of NE projections may mediate behavioral improvement.

Introduction

Major depressive disorder (MDD) is a pervasive mental illness with the greatest global lifetime disability (WHO, 2017), yet it remains poorly understood. MDD is thought to involve reduced serotonin (5-HT) activity (Jans et al., 2007; Krishnan and Nestler, 2008; Warner-Schmidt, 2013; Booij et al., 2015), although the clinical data supporting this remain unclear. Serotonin reuptake inhibitors (SSRIs), which increase synaptic 5-HT, remain the first-line treatment (Kennedy et al., 2016; Artigas et al., 2018). However, SSRI treatment requires >4 weeks for clinical benefit,

and 60% of patients who do not remit are sequentially switched to other SSRIs or antidepressants targeting other monoamine systems (Trivedi et al., 2006; Rush et al., 2009) such as desipramine (DES), which primarily targets the norepinephrine (NE) transporter (NET) (Dziedzicka-Wasylewska et al., 2006). However, a rational treatment strategy is lacking, and repeated treatment failures occur in 30% of patients, who are classified as "treatment-resistant."

Response to SSRIs is associated with desensitization of 5-HT1A autoreceptors in rodent models of depression (Le Poul et al., 2000; Riad et al., 2004, 2017; Rainer et al., 2012), as well as in SSRI-treated MDD subjects (Gray et al., 2013). The 5-HT1A autoreceptor is a major negative regulator of 5-HT activity and downregulation of the receptor correlates with enhanced 5-HT release (Albert and Lemonde, 2004; Albert et al., 2011; Garcia-Garcia et al., 2014), resilience to stress, and accelerated and augmented response to SSRI treatment (Richardson-Jones et al., 2010). In humans, the rs6295 5-HT1A promoter polymorphism leads to increased transcription of the 5-HT1A gene in 5-HT cells (Lemonde et al., 2003; Jacobsen et al., 2008) and has been associated with increased raphe 5-HT1A autoreceptor levels in depressed subjects compared to controls (Parsey et al., 2006, 2010; Hesselgrave and Parsey, 2013), but reductions in cortical 5-HT1A postsynaptic receptors (Donaldson et al., 2016; Kautzky et al., 2017). Postmortem studies of depressed suicide brains have also shown increased levels of dorsal raphe (DR) 5-HT1A autoreceptors compared to control brains (Stockmeier et al., 1998; Boldrini et al., 2008). Together, these results suggest that excessive inhibition of 5-HT activity by an increase in 5-HT1A autoreceptors may contribute to resistance to SSRI treatment.

To address the role of 5-HT1A autoreceptors in antidepressant response, we conditionally knocked out the 5-HT1A gene repressor Freud-1/CC2D1A in 5-HT neurons of adult mice, generating cF1ko mice (Vahid-Ansari et al., 2017). The cF1ko mice display increased 5-HT1A autoreceptor binding and function and reduced raphe 5-HT levels and activity resulting in an SSRI-resistant depression and anxiety phenotype (Vahid-Ansari et al., 2017). We have used these mice to address which antidepressants are effective when genetic variation reduces the activity of the 5-HT system.

We hypothesized that antidepressants targeting non-5-HT systems may improve behavior in the SSRI-resistant cF1ko mice (Vahid-Ansari et al., 2019). Thus, the cF1ko mice were treated with DES to increase the activity of the NE system (Tremblay and Blier, 2006). We found that in contrast to SSRI treatment, the cF1ko mice responded to chronic DES treatment in multiple validated anxiety and depression tests. To address the NE-mediated mechanisms involved in DES response, we examined brain-wide changes in FosB+ cells as an index of chronic cellular activity (Nestler, 2015). We also examined changes in NE innervation by quantifying NET+ axonal volume and varicosity number (Belmer et al., 2017; Zahrai et al., 2020). To visualize NE synapses with glutamate or GABA neurons, we quantified NET-synaptophysin pre-synapses located proximal (<0.6 μm) to PSD95- or gephyrin-labeled postsynaptic densities, respectively. We found reduced NE varicosity density and NE synapses in the cF1ko mice compared to WT mice, and DES treatment reversed these deficits to WT levels. We propose that DES induces a novel mechanism of region-specific NE reinnervation to restore NE activity and mediate behavioral recovery in SSRI-resistant cF1ko mice. These studies suggest a rational approach to the clinical treatment of SSRI resistance: in patients with reduced 5-HT activity, antidepressants targeting other monoamines may be effective (Blier and El Mansari, 2013).

Material and Methods

Mouse models
The University of Ottawa Animal Care Committee, in accordance with the Canadian Council on Animal Care, approved all animal protocols, and both sexes of mice were used. Animals were maintained on a 12 h light/dark cycle (7:00 A.M. to 7:00 P.M.) with ad libitum access to food and water. The cF1ko mice were generated by crossing CC2D1A (Freud-1)$^{flx/flx}$ mice with TPH2-CreERT2 mice (stock#016584, C57BL/6N background, Jackson Laboratory; Vahid-Ansari et al., 2017). TPH2-CreERT2-Freud-1flx/flx (**cF1ko**) and TPH2-CreERT2-Freud-1 wt/wt (**WT**) littermates were examined. As described previously, at 8–9 weeks of age, CreERT2 was activated using three injections of tamoxifen [180 mg/d (~3 mg/kg), i.p., Sigma #T5648] over 5 d, which induces a 50% increase in 5-HT1A receptor binding specifically in 90% of 5-HT cells (Vahid-Ansari et al., 2017). Mice were treated with 160 mg/L DES (Sigma D3900) in drinking water (Santarelli et al., 2003). Fluid consumption was not different between water at 5.08 ± 0.6 ml/d ($n = 21$, 11 WT + 10 cF1ko) and DES at 5.36 ± 0.2 ml/d ($n = 19$, 10 WT + 9 cF1ko) for a final DES concentration of ~20 mg/kg/d. Treatment was done for 3 weeks and during subsequent behavior analyses.

Genotype analysis. At 3 weeks of age, ear punches were obtained from all mice, and DNA was extracted using the REDExtract-N-Amp Tissue PCR kit (Sigma). PCR was done using the following primers (Table 1) and conditions: for CC2D1A$^{flx/flx}$, cc2-5′ nf: 5′-TAG AAA CAC TTA CCC TCC ACA TTG-3′and cc2-3′sh: 5′-TAG GAA GTG CCC ACC CAG A-3′. The PCR conditions were as follows: 94°C, 4 min; 15 cycles at 94°C, 30 s; 70°C, 30 s, −0.5°C/cycle; and 72°C, 30 s and then 20 cycles at 94°C, 30 s; 62°C, 30 s; 72°C, 30 s; 72°C, 10 min; and 10°C. This protocol results in 202 bp (WT) and 382 bp (cF1ko) products detected using a green dye master mix (New England Biolabs). The following are the primers used for TPH2-CreERT2: TPH2-11679: 5′-GCT GAG AAA GAA AAT TAC ATC G-3′, CRE-12523: 5′-TGG CTT GCA GGT ACA GGA GG-3′, OIMR8744: 5′-CAA ATG TTG CTT GTC TGG TG-3′, and OIMR8745: 5′-GTC AGT CGA GTG CAC AGT TT-3′. The PCR conditions were as follows: 94°C, 1 min; 35 cycles at 94°C, 15 s; 57°C, 20 s; 72°C, 10 s; 72°C, 2 min; and 10°C. This protocol results in 200 bp (WT) and 300 bp (transgenic) products using easy Taq DNA polymerase (TransGen Biotech, Civic Bioscience).

Behavioral tests
Behavioral tests were conducted following the timeline shown in Figure 1. Mice were housed under normal light conditions, and tests were performed beginning at 10:00 AM, after at least 1 h of habituation to the testing room. Testing was performed under white light illumination except for the forced swim test (FST), which was performed under red light. Throughout testing and behavioral analyses, the experimenter was blind to the mouse genotype. In experimental groups, no differences between male and female mice were observed in the tests; therefore, the data were pooled.

Elevated plus maze test. The mice were placed in the center of an elevated two-arm plus maze, measuring $20 \times 6 \times 75$ cm^3 (Noldus) with one arm open and the other closed, with overhead illumination (100–110 lux) and a camera. Mice were placed in the center of the maze and explored the maze for 10 min. The mouse movements were tracked and the time spent in closed and open arms was determined (EthoVision XT 11.5, Noldus IT, RRID: SCR_000441).

Open field (OF) test. The mice were placed in a corner of the arena ($45 \times 45 \times 45$ cm) and explored the new environment for a total of 10 min at light levels of 300 lux. Mouse movements were videotaped, and the time spent on the outside of the center (24×24 cm^2) of the OF arena was analyzed (EthoVision XT 11.5).

FST. Each mouse was placed into a clear plastic cylinder 22 cm in diameter × 37 cm high and filled with water (24°C). The mouse

Table 1. Materials for genotyping

Reagent type	Designation	Source or reference	Identifiers	Additional information
Genetic reagent (*Mus musculus*)	CC2D1A	C. Manzini PMID: 26826102	Strain code: CRL:027; RRID: IMSR_CRL:027	
Genetic reagent (*Mus musculus*)	TPH2-CreERT2 (Tg(Tph2-icre/ERT2)6Gloss/J)	Jackson Lab MGI: 5049908 PMID:19936315	Stock #: 016584; RRID: IMSR_JAX:016584	
Commercial assay or kit	Extraction solution *	Millipore Sigma	Catalogue #: E7526–24 ml	* REDExtract-N-Amp Tissue PCR kit
Commercial assay or kit	Tissue preparation solution *	Millipore Sigma	Catalog #T3073—30 ml	* REDExtract-N-Amp Tissue PCR kit
Commercial assay or kit	neutralization solution *	Millipore Sigma	Catalog #N3910—24 ml	* REDExtract-N-Amp Tissue PCR kit
Sequence-based reagent	CC2D1A primer, cc2-5′NF 5′-TAG AAA CAC TTA CCC TCC ACA TTG-3′	PMID: 26826102		
Sequence-based reagent	CC2D1A primer, cc2-3′ sh. 5′-TAG GAA GTG CCC ACC CAG A-3′	PMID: 26826102		
Sequence-based reagent	TPH2-CreERT2 primer, TPH2-11679 5′-GCT GAG AAA GAA AAT TAC ATC G-3	PMID: 29636529		
Sequence-based reagent	TPH2-CreERT2 primer, CRE-125235′-TGG CTT GCA GGT ACA GGA GG-3′	PMID: 29636529		
Sequence-based reagent	TPH2-CreERT2 primer, OIMR8744 5′-CAA ATG TTG CTT GTC TGG TG-3′	PMID: 29636529		
Sequence-based reagent	TPH2-CreERT2 primer, OIMR8745 5′-GTC AGT CGA GTG CAC AGT TT-3	PMID: 29636529		
Other	Taq PCR master mix (green dye)	New England Biolabs	Catalog #M04896L	
Other	Easy Taq DNA polymerase	TransGen Biotech (Civic Bioscience)	Catalog #AP111	

movement was videotaped to measure the duration of immobility time for 6 min under red light illumination using an automated video tracking software from Med Associates (EthoVision XT 11.5).

Tail suspension (TS) test. The tail of the mouse was securely taped to a vertical bar, and the mouse was suspended for 6 min in TS boxes (Med Associates). An automated detection device (ENV-505TS Load Cell Amplifier) was used to determine immobility time through Med Associates software (EthoVision XT 11.5).

Novelty-suppressed feeding test. Animals were food-deprived for 16 h. After a brief habituation in a new cage, animals were individually placed in an arena (45 × 45 × 45 cm; 300 lux) with a food pellet placed in the center. The latency of the mouse to attempt eating food was recorded manually within 10 min. The mice were placed in their home cage, and the latency to approach the food and the amount of food consumed in 5 min were measured.

Immunofluorescence
FosB-, CamKIIα-, GAD67-, VGLuT1- or VGLuT3-, and TH-positive neuronal cells. Tissues were collected 24 h after the last behavioral test to reduce acute activation due to the last test and were compared to controls under the same conditions. Mice were anesthetized by lethal injection (0.01 ml/g, i.p.) of sodium pentobarbital (Somnitol; MTC Pharmaceuticals) and perfused by cardiac infusion of 30 ml PBS and then 25 ml 4% paraformaldehyde. Whole brains were isolated, cryoprotected overnight in 20% sucrose, and frozen at −80°C. Coronal brain slices (25 μm) were prepared using the coordinates summarized in Table 2 (Paxinos and Franklin, 2001). Slices were thaw-mounted on Superfrost slides (Thermo Fisher Scientific) and kept at −80°C. The sections were washed in PBS (3 × 10 min), blocked 1 h in PBS with 1% BSA, 10% NDS, and 0.1% Triton X-100, and incubated overnight at 4°C with primary antibodies (Table 3). The sections were then washed in PBS (3 × 10 min) and incubated for 1 h in the mixture of related secondary antibodies (Table 3) and 4′,6-diamido-2-phenylindole (DAPI, Thermo Fisher Scientific #D1406, RRID AB_2629482, 1:10,000) at 22°C. During analysis, a coding system was used so that the counter was blind to the treatment.

FosB immunofluorescence. To quantify FosB+ cell number, images of different brain areas (Table 2) were acquired with the AxioVision imaging software on a Zeiss Axio Observer D1 microscope ($n = 4$/group). The number of cells co-stained for FosB and DAPI (nuclear FosB when colocalized) was counted on images taken under 20× magnification of 25 μm slices. FosB+ staining colocalized with GAD67 or CaMKIIα was counted as FosB/GAD67+ or FosB/CaMKIIα+ for forebrain cells. FosB+ cells were quantified per area/section, and the mean values were then averaged. For DR, FosB/VGLuT3+ and FosB/GAD67+ cells were quantified. For locus coeruleus (LC), FosB/TH+, FosB/VGLuT1+, and FosB/GAD67+ cells were quantified. Positively stained cells were manually counted within a standardized template (134.95 × 134.95 μm) using ImageJ 1.48 version software (RRID: SCR_003070).

NET immunofluorescence. To quantify NE innervation, immunofluorescence was done for NET at dilution indicated in Table 3. Sections (25 μm) were incubated at 22°C for 1 h in blocking solution (4% normal goat serum, 1% BSA, 0.3% Triton X-100%, and 0.05% Tween20 in PBS) and then with rabbit anti-NET and mouse anti-PSD95 diluted in blocking solution for 24 h at 4°C. The sections were then washed with blocking solution (3 × 10 min) and incubated in goat anti-rabbit Alexa488 and goat anti-mouse Cy5 diluted in blocking solution (4 h, 22°C). The sections were then washed in blocking solution and PBS (3 × 10 min each), incubated in a mixture of normal rabbit (10%) and mouse (5%) sera in blocking solution for 1 h at 22°C, and finally washed with blocking solution (3 × 10 min). The sections were then incubated in goat anti-mouse and goat anti-rabbit monovalent *F*(ab) antibody fragments diluted in PBS and agitated for 1 h at 22°C. Monovalent antibody *F*(ab) fragments were used to block exposed immunoglobulins on the sections stained for triad formations with multiple primary antibodies from the same species (Belmer et al., 2017). The sections were then washed in blocking solution (3 × 10 min); stained with a mixture of mouse anti-synaptophysin and rabbit anti-gephyrin, which was diluted in blocking solution (24 h, 4°C); and washed in blocking solution (3 × 10 min). The sections were then incubated in a mixture of goat anti-mouse Alexa405 and goat anti-rabbit Alexa555 (1/1,000) diluted in a blocking solution (4 h, 22°C). The sections were then washed in blocking solution and PBS (3 × 10 min each) and imaged as described below.

Table 2. Coordinates relative to bregma of areas assessed by immunofluorescence

Brain area	CG	PL	IL	NAc	LSN	CA1	CA2/3	DG	BLA	DR	EC	LC
Bregma (mm)	1.7	1.7	1.7	1.1	0.5	−1.7	−1.7	−1.7	−2.06	−4.72	−4.72	−5.4

CG, cingulate cortex; PL, prelimbic; IL, infralimbic; NAc, nucleus accumbens; LSN, lateral septal nucleus; CA1, CA2/3, hippocampal regions; DG, dentate gyrus; DR, dorsal raphe; EC, entorhinal cortex; LC, locus coeruleus.

Table 3. Primary/secondary antibodies used for immunofluorescence staining

	Host	Dilution	Company	Catalog #	RRID
Primary antibody					
CaMKIIα	G	1/250	Thermo Fisher Scientific	PA5-19128	AB_10986857
FosB	R	1/500	Santa Cruz Biotechnology	sc-48	AB_631515
FosB	M	1/500	Abcam	ab11959	AB_298732
GAD 67	M	1/500	Millipore Sigma	MAB5406	AB_2278725
Gephyrin	R	1/1000	Abcam	ab32206	AB_2112628
NET	R	1/300	Synaptic Systems	260,003 (SY)	AB_2619974
PSD95	M	1/1000	Abcam	ab2723	AB_303248
Synaptophysin	M	1/500	Millipore Sigma	MAB5258	AB_95185
TH	R	1/1000	Millipore Sigma	AB152	AB_390204
VGLuT1	GP	1/100	Millipore Sigma	AB5905	AB_2301751
VGLuT3	GP	1/100	Millipore Sigma	AB5421-I	AB_2819014
Secondary antibody					
Anti-rabbit 488	G	1/1000	Thermo Fisher Scientific	A11034	AB_2576217
Anti-mouse 405	G	1/100	Thermo Fisher Scientific	A-31553	AB_221604
Anti-mouse Cy5	G	1/1000	Abcam	AB6563	AB_955068
Anti-rabbit 555	G	1/1000	Thermo Fisher Scientific	A-21428	AB_2535849
Anti-guinea pig cy5	D	1/250	Jackson ImmunoResearch Laboratories	706-175-148	AB_2340462
Anti-mouse cy3	D	1/250	Jackson ImmunoResearch Laboratories	715-165-150	AB_2340813
Anti-rabbit 488	D	1/1000	Thermo Fisher Scientific	A-21206	AB_2535792
Anti-guinea pig 594	G	1/200	Thermo Fisher Scientific	A-11076	AB_2534120
Anti-rabbit 594	G	1/200	Abcam	A-11037	AB_2534095
Monovalent F(ab) (anti-rabbit)	G	1/100	Jackson ImmunoResearch Laboratories	115-007-003	AB_2338476
Monovalent F(ab) (anti-mouse)	G	1/100	Jackson ImmunoResearch Laboratories	111-007-003	AB_2337925

Imaging for triadic synapses with NET-positive axons. Images (1,024 × 1,024 pixels) were acquired using confocal laser scanning on a Zeiss LSM880 AxioObserver Z1 microscope with a Zeiss AxioObserverZ1 mot inverted stand fitted on an IX83 automated inverted platform with a Plan Apochromat oil-immersed 63× objective lens (1.4 NA) and solid-state lasers (405, 488, 561, and 639 nm) at an exposure of 0.42 μs/pixel and z spacing of 0.3 μm. The region of interest template size (μm) was 134.95 × 134.95 × 15.6 ($n = 4$/group). Channels were sequentially scanned to avoid any overlap in excitation/emission wavelengths (405/639 and 488/561 nm). Images were taken using the ZenBlack 2.3 software. This led to a pixel size of 0.13 μm and a resolution limit of 145 μm according to Abbe's law (Wang and Smith, 2012). The channels were mostly imaged sequentially using the adjustable emission band path to avoid any bleeding through. First, the Alexa 555 was excited by the laser diode 561 nm, and the emission band path was set at 569–657 nm. Alexa 488 nm was visualized using the Argon laser, 480 nm line, and emission band path: 493–604 nm. Alexa 405 and Alexa 647 were then imaged simultaneously, with the HeNe 633 nm laser and the diode 405 nm laser combined with the emission band path set at 410–501 nm and 638–745 nm, respectively. To compensate for light scattering and the point spread function (PSF), acquired images were deconvolved using AutoQuant X3.1 software with 10 iterations, high noise level, adaptive PSF, theoretical PSF, and a refractive index value for the objective lens' immersion medium of 1.515. A correction for the distance from the coverslip was also applied where the length of the unblurry region of the Y–Z plane was measured (4–8 μm) and entered for three-dimensional deconvolution. To maintain the x/y/z voxel size, each deconvolved image was saved as an Imaris file (Bitplane IMS 5 file).

Image analysis using Imaris x64 9.1.2 for synaptic triad formations. Analysis with Imaris was done as previously described (Schatzle et al., 2012; Fogarty et al., 2013; Klenowski et al., 2015). NET immune-labeled

fibers were reconstructed in 3D with Imaris' surface rendering function, and axonal volume density was calculated. Imaris' masking function was then used to remove intra-fiber labeling and conserve the fluorescently tagged synaptophysin, gephyrin, and PSD95 located outside of the NET surfaces made previously (Syn[out], Geph[out], and PSD95[out], respectively). This was then used to mark putative inhibitory (gephyrin) and excitatory (PSD95) neurochemical synapses. Also, removing synaptophysin's fluorescence signal outside of the created NET surfaces ensured that only synaptophysin within the NET+ fibers was being identified, and putative noradrenergic synaptic boutons (SYN[NET+]) were then quantified. Imaris's spot detection tool was then applied to each of the constructed masks with noradrenergic boutons marked as Syn[NET+], inhibitory synapses as Syn[NET+]/Geph[out], and excitatory synapses as Syn[NET+]/PSD95[out] for detection of spots within a diameter of 0.6 μm. This size was selected based on the Z step-size to ensure that spots were present in a minimum of two confocal optical slices and that spots are present in 3D space and are not just artifacts from Imaris, as previously described (Fogarty et al., 2013; Klenowski et al., 2015). Imaris's spot colocalization tool was then used to label either Syn[NET+]/Geph[out] or Syn[NET+]/PSD95[out] spot pairs, within 0.6 μm between spots within a pair, to identify pairs of putative inhibitory or excitatory synapses, respectively. Syn[out] boutons that were located within 0.6 μm of Syn[NET+]/Geph[out] (putative inhibitory synapse) or Syn[NET+]/PSD95[out] (putative excitatory synapse) spots pairs were also labeled as adrenergic inhibitory and excitatory triads, respectively (Belmer et al., 2017). NET+ fibers were reconstructed using Imaris's filament tool, with the filament diameter being 0.5–0.6 μm, and the axonal volumes were determined using surface reconstruction of the axons. A minimal ratio of branch length to trunk radius of 1.5–2.5 to reduce the background signal, with further filter processing was done to remove artificial fibers. The length and volume of NET+ axons were then determined. The number of NET+ varicosities was also determined using the spot detection tool in Imaris, with spots of varying sizes fitted into corresponding varicosities.

Statistical analysis

The data were plotted and analyzed using the Statistical Package for the Social Sciences (GraphPad Prism version 9.4.1 for Windows, GraphPad Software; www.graphpad.com, RRID: SCR_002798). Data are expressed as mean ± SEM. Since no sex difference was seen, data from both sexes were pooled. Images from four mice were averaged for each brain region. *Two-way ANOVA was performed for comparing WT, cF1ko, WT + DES, and cF1ko + DES groups, with significance being set at p < 0.05. Post hoc comparisons were also made with Tukey's multiple comparison test.*

Results

Chronic DES treatment restores behavioral phenotypes in cF1ko mice

The effect of chronic treatment with DES on behavior was examined, comparing both sexes of cF1ko mice and WT (WT) littermates. The mice received tamoxifen injections at 8 weeks of age (Fig. 1A), initiating CreERT2-mediated knockout of the Freud-1 gene in 5-HT neurons, shown to induce 5-HT1A autoreceptor expression and reduce 5-HT activity (Vahid-Ansari et al., 2017). Treatment with DES (20 mg/kg in drinking water) or vehicle (V) was started at 11 weeks and continued throughout

behavioral testing. In the elevated plus maze (EPM) test, a significant treatment × genotype effect was seen, with cF1ko spending 50% less time in the open arms than WT mice with no difference in closed arm time (Fig. 1B). No differences in total distance traveled were seen (data not shown) indicating that change in open arm time was not due to altered locomotor activity, consistent with anxiety-like behavior. In the OF test, cF1ko mice spent significantly less time (about 50%) in the center of the arena (Fig. 1C). Thus, the cF1ko mice showed consistent anxiety-like behavior. Depression-like behavior was also detected in the cF1ko versus WT mice, with increased immobility in FST (Fig. 1D) and TS tests (Fig. 1E). Similarly, in the novelty-suppressed feeding (NSF) test, the cF1ko mice displayed significantly greater latency to feed compared to WT mice, whereas no difference was observed in feeding latency (Fig. 1F) or food consumption (data not shown) in the home cage, again consistent with an anxiety-like phenotype. These data indicate that the knockout of Freud-1 in 5-HT neurons during adulthood in the cF1ko mice is sufficient to induce both anxiety- and depression-like phenotypes (Vahid-Ansari et al., 2017).
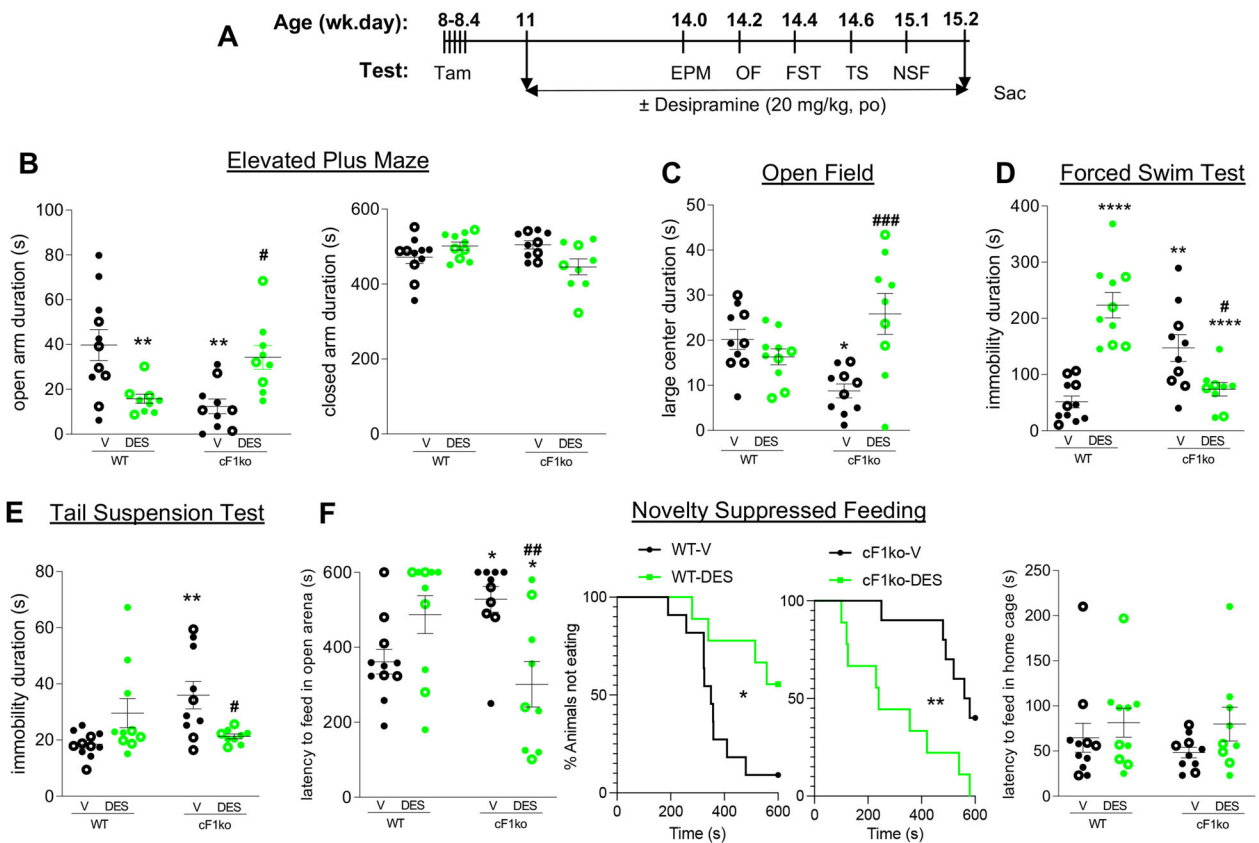

Figure 1. Chronic DES treatment reverses anxiety- and depression-like behaviors in cF1ko mice. WT or cF1ko mice were treated with DES, 20 mg/kg, per oral or vehicle (V) for 3 weeks and throughout the behavioral assays (*A*, timeline). Data from male (filled dots) and female (open dots) mice are shown and plotted as mean ± SEM. *B*, *C*, Anxiety phenotype: chronic DES reduced anxiety in cF1ko mice. *B*, EPM, significant changes in time spent in open arms in EPM test (two-way ANOVA treatment × genotype interaction, $F_{(1,36)} = 21.63$; $p < 0.0001$). Data show **$p < 0.01$ versus WT-V and #$p < 0.05$ versus cF1ko-V, Tukey's post hoc test. *C*, OF, changes in distance traveled in the large center (two-way ANOVA treatment × genotype interaction, $F_{(1,36)} = 12.4$; $p = 0.0011$). Data show *$p < 0.05$ versus WT-V and #$p < 0.05$ versus cF1ko-V, Tukey's post hoc test. *D*, *E*, Depression phenotype. *D*, FST, depression-like behavior in WT (V) compared to WT (DES) as indicated by increased immobility in the FST. Chronic DES significantly reduced immobility in *cF1ko* mice (two-way ANOVA treatment × genotype interaction, $F_{(1,36)} = 44.98$; $p < 0.0001$). Data show ****$p < 0.0001$ versus WT-V and #$p < 0.05$ versus cF1ko-V, Tukey's post hoc test. *E*, TST, chronic DES significantly reduced immobility in cF1ko mice (two-way ANOVA treatment × genotype interaction, $F_{(1,36)} = 12.24$; $p = 0.0013$). Pairwise comparison **$p < 0.01$ versus WT-V and #$p < 0.05$ versus cF1ko-V, Tukey's post hoc test. *F*, NSF, the left panel shows latency to approach food in the novel arena (two-way ANOVA treatment × genotype interaction, $F_{(1,36)} = 17.08$; $p = 0.0002$). *$p < 0.05$ versus WT-V; ##$p < 0.01$ versus cF1ko-V, Tukey's post hoc test. Survival curves show the time to first approach to food pellet for WT or cF1ko mice (middle panels). Kaplan–Meier analysis showed a significant difference by Mantel–Cox log-rank test for WT, $\chi^2 = 6.467$, df = 1, *$p = 0.011$ and cF1ko $\chi^2 = 8.149$, df = 1, **$p = 0.0043$. The right panel shows latency to approach food in the home cage, two-way ANOVA $F_{(1,36)} = 0.2539$, $p = 0.6174$. Data represent results from individual animals with mean ± SEM; $n = 9–11$/group.

A significant effect of chronic DES compared to vehicle treatment was also seen but differed between WT and cF1ko mice. Unexpectedly, in the EPM test, chronic DES treatment in WT mice reduced open arm time but had no significance in the OF test compared to vehicle (Fig. 1B,C). Kaplan–Meier analysis of NSF data also showed an increased latency to feed in DES-treated WT mice (Fig. 1F), indicating a test-dependent anxiogenic action of DES in WT mice. In WT mice, DES also significantly increased immobility in FST, with a trend in TS (Fig. 1D,E), suggesting a partial pro-depressive action. Conversely, in cF1ko mice, DES significantly increased open arm time in EPM, reduced latency to feed in the NSF test, and increased time in the center in the OF, reversing the anxiety-like phenotype of cF1ko mice to levels seen in vehicle-treated WT mice (Fig. 1B,C,F). Compared to vehicle, chronic DES treatment also significantly reduced the immobility duration of cF1ko mice in the FST and TST to levels seen in vehicle-treated WT mice

(Fig. 1D,E). These results indicate that, while SSRI was ineffective (Vahid-Ansari et al., 2017), chronic DES treatment reverses the anxiety- and depression-like phenotypes seen in the cF1ko mice.

Chronic DES treatment induces recovery of cellular FosB levels in cF1ko mice

To address brain activity changes that might underlie the observed behavioral changes, brain sections of corticolimbic areas and midbrain raphe and LC (Fig. 2A) were obtained after behavioral tests, immunostained for FosB as a marker of chronic cellular activation (Nestler, 2015; Vialou et al., 2015), and the number of FosB-labeled cells was quantified. It should be noted that both acute- and chronic-expressed forms of FosB are detected and could reflect in part experience-dependent changes. Regions examined included 5-HT projection areas with detectable FosB-labeled cells counted at coordinates described in Materials and Methods. Based on different behavioral actions
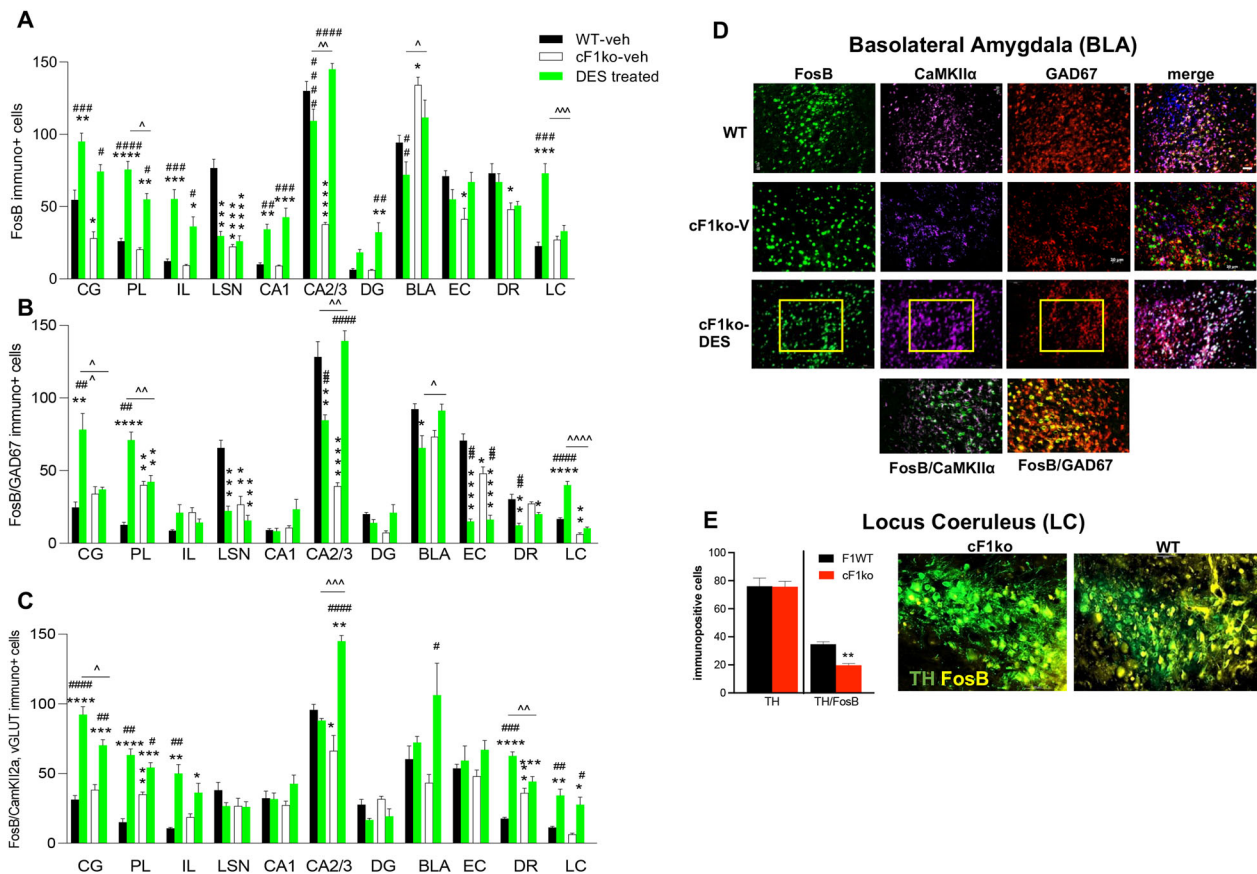

Figure 2. DES-induced changes in cellular activity in cF1ko versus WT mice. Immunofluorescence for FosB, GAD67, and CaMKIIα was done on brain sections from WT or cF1ko mice treated with DES or vehicle (veh) obtained after behavioral testing (Fig. 1A, timeline). *A–C*, Quantification of FosB+ (*A*), FosB/GAD67+ (*B*), and FosB/CaMK IIα+ (*C*) cell counts (representative images shown in *D*). Data represent results from individual animals with mean ± SEM ($n = 3$ mice/group). Data from brain regions were analyzed by two-way ANOVA (for *A–C*). **A-FosB**: CG = cingulate cortex, $F_{(1,8)} = 0.2937$, $p = 0.6026$; PL = prelimbic, $F_{(1,8)} = 4.201$, $p = 0.0745$; IL = infralimbic, $F_{(1,8)} = 2.884$, $p = 0.1279$; LSN = lateral septum, ***$F_{(1,8)} = 39.70$, $p = 0.0002$; hippocampal subregions—CA1, $F_{(1,8)} = 1.658$, $p = 0.2339$, and CA2/3, ****$F_{(1,8)} = 129.1$, $p < 0.0001$; DG = dentate gyrus, $F_{(1,8)} = 4.402$, $p = 0.0691$; BLA = basolateral amygdala, $F_{(1,8)} = 5.800e{-}030$, $p > 0.9999$; EC = entorhinal cortex, **$F_{(1,8)} = 14.15$, $p = 0.0055$; DR = dorsal raphe, $F_{(1,8)} = 1.180$, $p = 0.3091$; LC = locus coeruleus, ***$F_{(1,8)} = 26.40$, $p = 0.0009$. **B-FosB/GAD67**: CG, **$F_{(1,8)} = 16.06$, $p = 0.0039$; PL, ****$F_{(1,8)} = 52.95$, $p < 0.0001$; IL, $F_{(1,8)} = 7.841$, *$p = 0.0232$; LSN, **$F_{(1,8)} = 12.73$, $p = 0.0073$; CA1, $F_{(1,8)} = 3.354$, $p = 0.1044$; CA2/3, ****$F_{(1,8)} = 115.5$, $p < 0.0001$; DG, *$F_{(1,8)} = 10.06$, $p = 0.0132$; BLA, **$F_{(1,8)} = 16.03$, $p = 0.0039$; EC, *$F_{(1,8)} = 10.49$; $p = 0.0119$; DR, *$F_{(1,8)} = 6.966$, $p = 0.0297$; LC, ***$F_{(1,8)} = 43.13$, $p = 0.0002$. **C-FosB/CaMKIIα**: CG, **$F_{(1,8)} = 12.11$, $p = 0.0083$; PL, **$F_{(1,8)} = 20.57$, $p = 0.0019$; IL, $F_{(1,8)} = 5.140$, $p = 0.0531$; LSN, $F_{(1,8)} = 1.340$; $p = 0.2804$; CA1, $F_{(1,8)} = 2.779$, $p = 0.1341$; CA2/3, ****$F_{(1,8)} = 47.61$, $p = 0.0001$; DG, $F_{(1,8)} = 0.03695$, $p = 0.8524$; BLA, *$F_{(1,8)} = 6.426$, $p = 0.0350$; EC, $F_{(1,8)} = 0.9650$, $p = 0.3547$; DR, ***$F_{(1,8)} = 40.33$, $p = 0.0002$; LC, $F_{(1,8)} = 0.05543$, $p = 0.8198$. Significant differences by Tukey's post hoc test compared to saline (vehicle)-treated WT (*); veh-treated cF1ko (#); or between DES-treated WT and cF1ko (^); $p < 0.05$ (one symbol), 0.01 (two symbols), 0.001 (three symbols), 0.0001 (four symbols). *D*, Representative images of FosB, GAD67, and CaMKIIα staining in BLA showing reduced FosB/GAD67 (merge, yellow) and FosB/CaMKIIα (merge, white) colocalization in the template (boxed) of cF1ko versus WT mice, with recovery upon DES treatment. 2D images taken on inverted epifluorescent Z1 microscope (10× above, 20× below); scale bar, 50 and 20 μm. *E*, Representative images of FosB (yellow) and TH (green) staining in LC from WT and cF1ko mice. At the left is the quantification of TH and Fos/TH positive cell number. Data represent quantification of samples from individual animals as mean ± SEM; $n = 3$/group, analyzed by unpaired two-tailed t test ($t = 7.028$, df = 4), **$p < 0.01$ versus WT.

of DES in WT and cF1ko mice in some tests, we hypothesized that there would be genotype × treatment interactions on FosB expression in some brain areas, and this was the case (Fig. 2, legend). In other regions, similar actions of DES on FosB were observed in WT and cF1ko mice, consistent with the behavioral improvement seen in both genotypes.

Comparing total FosB+ cell counts in cF1ko to WT, widespread reductions were observed, most strongly in the lateral septal nucleus (LSN), hippocampal CA2/3, and entorhinal cortex (EC) (Fig. 2A). Chronic treatment with DES restored FosB+ cell counts in cF1ko mice to or above WT levels in hippocampus CA2/3 and EC. In LC, DES treatment increased the number of FosB+ cells in WT but not cF1ko mice. Oppositely, in LSN DES increased FosB+ cells in WT mice but had no effect in cF1ko mice, indicating a differential response to DES in cF1ko versus WT mice. Overall, these results show that DES treatment in cF1ko mice was effective in restoring normal total FosB activity in corticolimbic regions most impaired compared to WT mice, especially hippocampal CA2/3 and EC.

To identify the cell types activated, co-immunostaining for FosB with neuronal markers for glutamate/pyramidal cells (CaMKIIα, vGlut1 or vGlut3, Fig. 2B) or γ-aminobutyric acid (GABA) interneurons (GAD67, Fig. 2C) was quantified in brains from mice treated with vehicle or DES. Figure 2D shows a representative image of co-staining for FosB and CaMKIIα or GAD67 in the BLA. In the LC, TH staining was used to identify NE neurons (Fig. 2E). Comparing cF1ko to WT brains, in the BLA of cF1ko mice, the number of FosB+ CaMKIIα and GAD67 cells was similar to that in WT. In the LSN, EC, and partly CA2/3, the decrease in FosB in cF1ko versus WT mice was mainly in FosB/GAD67+ cells, suggesting a reduction in GABAergic activity in the EC-CA2/3 circuitry in cF1ko mice. In the DR, FosB/vGlut3+ cells were increased with no change in FosB/GAD67+ cells suggesting that the reduction in total FosB in DR may reflect reduced FosB/TPH+ cells due to increased 5-HT1A autoreceptor expression (Vahid-Ansari et al., 2017). In the LC, a decrease in FosB/GAD67+ as well as in FosB/TH+ cells was seen (Fig. 2E,F), with no change in FosB/vGlut1+ cells. Thus, in cF1ko versus
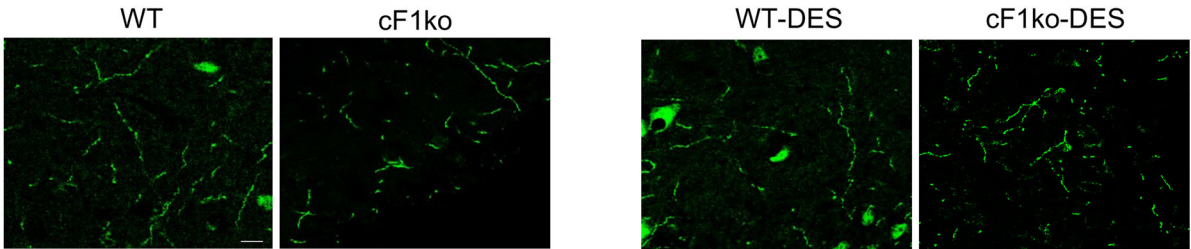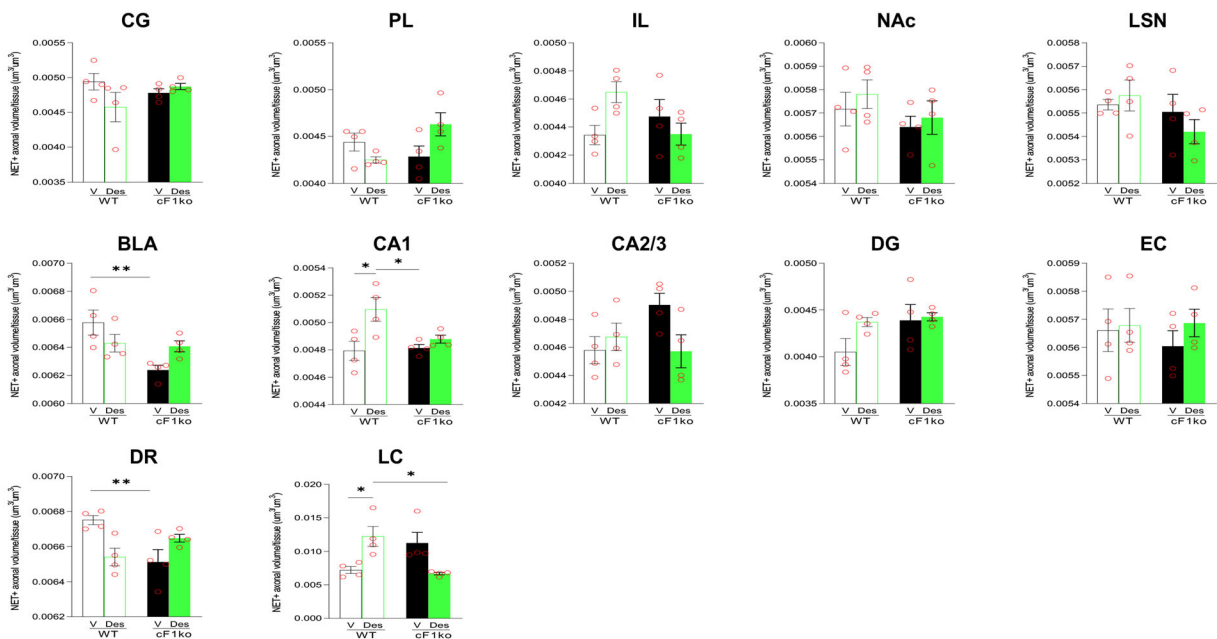
Figure 3. NET+ axonal volume changes in vehicle or DES-treated WT and cF1ko. Immunofluorescence for NET was done on brain sections from WT or cF1ko mice treated with DES or vehicle (V) obtained after behavioral testing (timeline, Fig. 1A). *A*, Chronic DES reverses the reduction in NE axonal volume in BLA of cF1ko. 2D images taken on an inverted epifluorescent Z1 microscope (20×) scale bar, 20 μm of NET-stained sections of the BLA in different conditions at 20× magnification. Scale bar, 20 μm. *B*, Quantification of NET+ axonal volume normalized to tissue volume. The density of NET+ axons was significantly reduced in BLA and DR of cF1ko versus WT and was partially rescued by DES treatment, while DES increased NET+ axons in CA1 and LC of WT but not cF1ko mice. Data were analyzed by two-way ANOVA: CG = cingulate cortex, $F_{(1,12)} = 3.280$, $p = 0.0952$; *PL = prelimbic, $F_{(1,12)} = 7.485$, $p = 0.0181$; *IL = infralimbic, $F_{(1,12)} = 5.948$, $p = 0.0312$; NAc = nucleus accumbens, $F_{(1,12)} = 0.03386$, $p = 0.8571$; LSN = lateral septum, $F_{(1,12)} = 1.173$, $p = 0.3001$; *BLA = basolateral amygdala, $F_{(1,12)} = 6.895$, $p = 0.0221$; hippocampal regions—CA1, $F_{(1,12)} = 4.084$, $p = 0.0662$, and; CA2/3, $F_{(1,12)} = 1.122$, $p = 0.3103$; DG, $F_{(1,12)} = 0.3423$, $p = 0.5693$; EC = entorhinal, $F_{(1,12)} = 1.356$, $p = 0.2669$; **DR = dorsal raphe, $F_{(1,12)} = 13.89$, $p = 0.0029$; **LC = locus coeruleus, $F_{(1,12)} = 18.09$, $p = 0.0011$. Data points (red circles) represent individual animals and shown are mean ± SEM; $n = 4$/group, *$p < 0.05$, **$p < 0.01$ by Tukey's post hoc test, as indicated.

WT mice, reduced GABAergic activity in the LC and EC-hippocampal circuitry, as well as in LSN, was seen. By contrast, FosB+ excitatory cells were not significantly altered in these areas in cF1ko versus WT mice.

The actions of chronic DES treatment on FosB+ cell types were examined in WT and cF1ko mice (Fig. 2). Strikingly, in the mPFC [cingulate cortex (CG), IL, PL] of cF1ko mice, DES strongly increased FosB in CaMKIIα+ cells with little or no effect in GABAergic cells, while in WT mice both were strongly increased. This indicates an overall activation of the mPFC by DES in cF1ko mice. In addition, in cF1ko but not WT mice, DES strongly induced excitatory (hippocampal CA2/3, BLA) and inhibitory neurons (CA2/3, DG, BLA), restoring their activity to or above WT levels. In several regions (LSN, CA1, DG, EC), FosB+ excitatory cells were not significantly altered by DES treatment in cF1ko or WT mice, which reduced FosB+ inhibitory cells in LSN (WT only) and EC. In the DR, DES-induced increase in FosB/vGlut3+ cells was blunted in cF1ko compared to WT mice, consistent with 5-HT1A-induced inhibition of vGlut3 neurons in these mice (Vahid-Ansari et al., 2017). By contrast, DES-induced FosB/vGlut1+ cells were equally in the LC of both WT and cF1ko mice; however, the activation of interneurons in the LC was blunted in the cF1ko mice. In summary, the adverse actions of

DES treatment on behavior in WT compared to cF1ko mice were associated with activation of inhibitory and CaMKIIα+ neurons in the mPFC and LC and with inhibition of interneurons in hippocampal CA2/3, LSN, and BLA. Conversely, the behavioral recovery induced by DES in cF1ko mice was associated with strong activation of inhibitory and excitatory neurons in hippocampal CA2/3 and BLA. The results in cF1ko mice and their reversal by DES treatment suggest a role for altered NE input in DES action.

Altered NE projections in cF1ko mice and rescue by DES treatment

We have previously shown that 5-HT and NE projections are altered in a mouse model of poststroke depression (Zahrai et al., 2020). To address whether NE projections are affected in cF1ko mice, NET immunofluorescence was used to detect NE axons and varicosities, as shown for BLA (Fig. 3A). The volume of NET+ processes and the density of NET+ varicosities were measured in a defined volume as we previously described (Zahrai et al., 2020). Only the DR and BLA showed a baseline alteration in NET+ axonal volume in cF1ko versus WT mice, with small but significant reductions that were reversed by chronic treatment with DES. Interestingly, there was a trend of

A. NET+varicosities in BLA-WT veh. treated
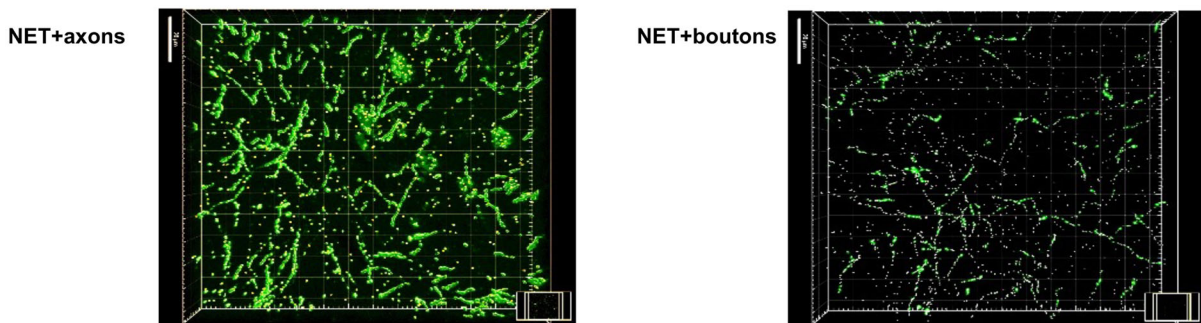
B. NET+ varicosities density
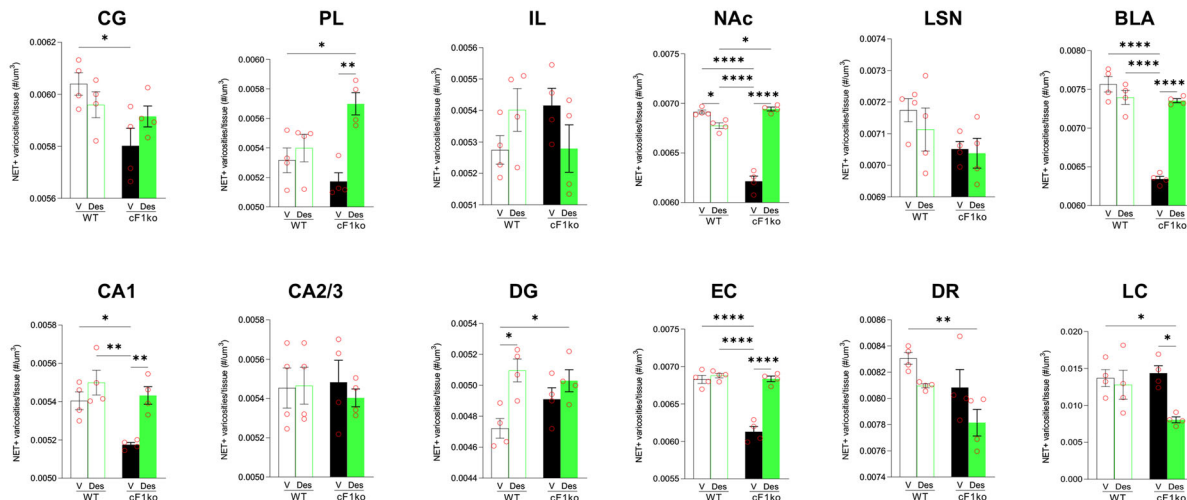
Figure 4. Reduced NET+ varicosity density in cF1ko versus WT mice and rescue by DES treatment. ***A***, Representative reconstructed flattened confocal images of NET-stained sections of the BLA from WT vehicle-treated mice are shown at 63× magnification with filtering for axons or varicosities. Scale bar, 20 μm. ***B***, Quantification of total number of NET+ varicosities normalized to tissue volume showing significant reductions of NE varicosities in cF1ko versus WT mice in NAc, BLA, and EC. DES induced recovery in these areas and an increase in PL of cF1ko mice. Abbreviations as in Figure 3. Data were analyzed by two-way ANOVA: CG, $F_{(1,12)} = 3.532$, $p = 0.0847$; *PL, $F_{(1,12)} = 7.902$, $p = 0.0157$; IL, $F_{(1,12)} = 4.577$, $p = 0.0537$; ****NAc, $F_{(1,12)} = 174.7$, $p < 0.0001$; LSN, $F_{(1,12)} = 0.2594$, $p = 0.6197$; CA1, $F_{(1,12)} = 3.062$, $p = 0.1056$; CA2/3, $F_{(1,12)} = 0.2485$, $p = 0.6272$; DG, $F_{(1,12)} = 3.249$, $p = 0.0966$; ***BLA, $F_{(1,12)} = 69.66$, $p < 0.0001$; ****EC, $F_{(1,12)} = 42.31$, $p < 0.0001$; DR, $F_{(1,12)} = 0.1125$, $p = 0.7431$; LC, $F_{(1,12)} = 4.609$, $p = 0.0529$. Data points (red circles) represent individual animals and shown are mean ± SEM; $n = 4$/group, *$p < 0.05$, **$p < 0.01$ by Tukey's post hoc test, as indicated.

increased axonal volume in cF1ko LC of twofold that was reduced by chronic DES, while in WT-DES significantly increased NET+ axonal density by twofold. Thus, the LC showed the highest density of NET+ axons and the largest fold changes in cF1ko or in response to DES treatment, while in most other regions, minimal or no changes were seen.

In addition to NE axons, NE varicosity density was visualized as presented in Figure 4A for BLA and quantified. In contrast to NE axonal density, much more widespread changes were seen in NET+ varicosity density in cF1ko versus WT mice (Fig. 4B). In cF1ko compared to WT mice, NET+ varicosity density was significantly reduced in NAc, BLA, and EC (by 10–15%) and weakly in PL (5%). These changes were reversed by chronic DES treatment, with induction above WT levels in PL and DG of cF1ko mice. In contrast, DES had little or no effect on NET+ varicosities in most regions of WT mice. Oppositely, in the LC of cF1ko but not WT mice, DES reduced varicosity density by 50%, consistent with the trend of reduced LC axonal volume (Fig. 3). The

reduction in LC varicosities may represent a compensatory adaptation of NE cells in cF1ko mice to DES blockade of reuptake of synaptic NE, possibly involving plasticity of pre-synaptic α_2-adrenergic autoreceptor signaling (Wagner-Altendorf et al., 2019). Taken together, these results suggest that suppression of 5-HT activity in cF1ko mice induces brain region-dependent deficits in NET+ axons and varicosities that can be partially or completely reversed by DES treatment.

Altered NE synapses and synaptic triads in cF1ko mice and rescue by DES

To specifically examine changes in NE synapses to inhibitory and excitatory synaptic sites, NET-synaptophysin co-immunofluorescence was used to label NE pre-synaptic sites (NET/Syn in), while proximal (<0.6 μm) PSD95+ or gephyrin+ postsynaptic sites (NET/Syn out) were quantified to assess NE synapses with inhibitory or excitatory synaptic sites, respectively. Figure 5, A and B, shows the representative images of reconstructed NET contacts
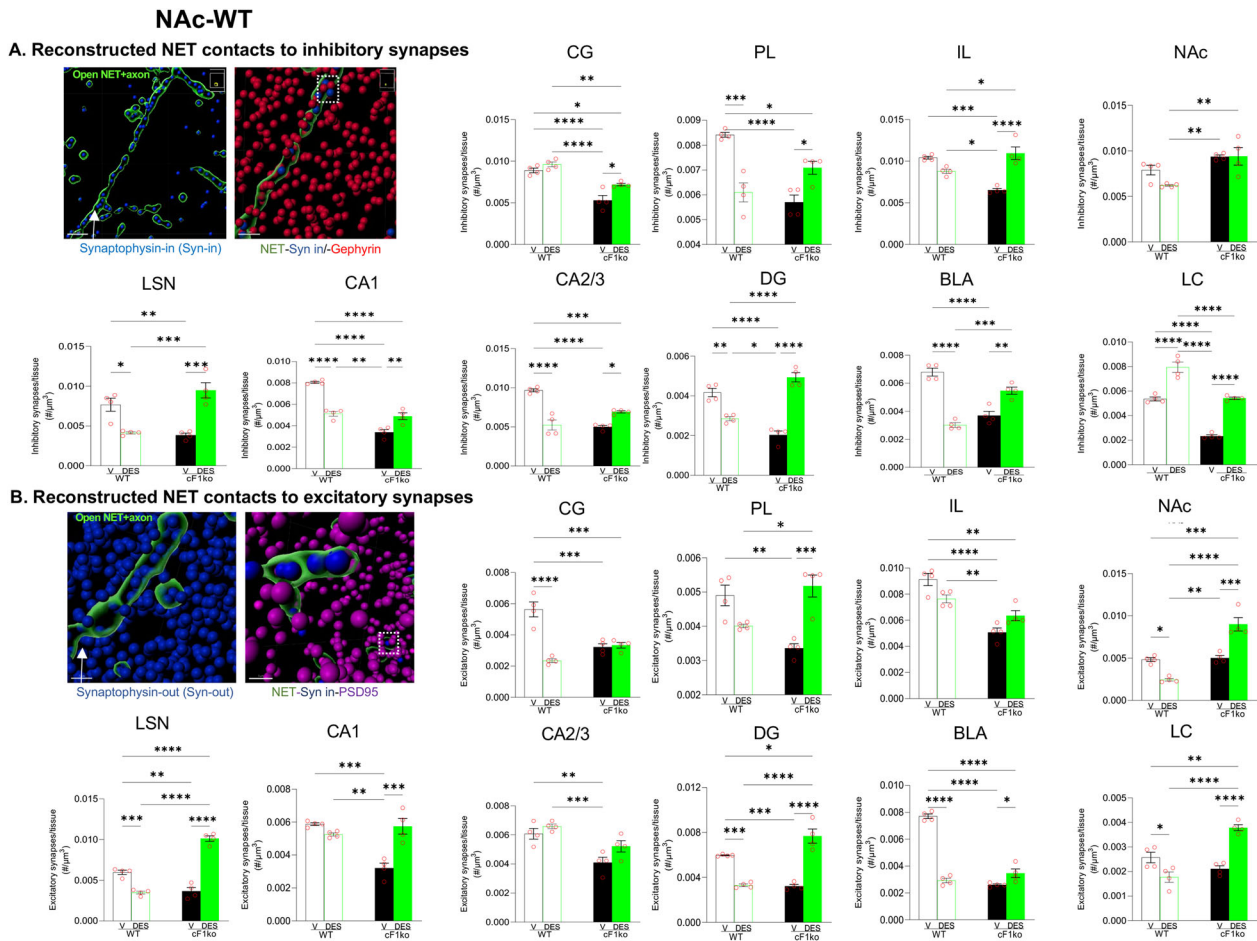
Figure 5. Chronic DES selectively reverses reductions of NET+ axonal synapse contacts in cF1ko. *A, B*, Representative reconstructed 63× confocal images of nucleus accumbens (NAc) from WT mice are shown co-stained for NET (green), synaptophysin (blue), and gephyrin (red) or PSD95 (purple) to visualize NE synapses with inhibitory and excitatory synapses (within 0.6 μm) (white boxes), respectively, distinct from non-NE synapses. Synaptophysin, gephyrin, and PSD95 boutons were reconstructed using Imaris software. Scale bar, 8 μm. NE synapses to excitatory and inhibitory synapses were quantified in brain regions of WT and cF1ko mice with DES or vehicle (V) treatment. For quantification of NE synapses to inhibitory synapses, sections were co-stained for NET, synaptophysin, and gephyrin; NET-synaptophysin+ boutons within 0.6 μm of gephyrin+ puncta were quantified and normalized to tissue volume. For quantification of NE synapses to excitatory synapses, sections were co-stained for NET, synaptophysin, and PSD95: NET-synaptophysin+ boutons within 0.6 μm of PSD95+ puncta were quantified and normalized to tissue volume. Data were analyzed by region using a two-way ANOVA. **A-NET/syn/geph**: CG, $F_{(1,12)} = 2.567$, $p = 0.1351$; PL, ****$F_{(1,12)} = 44.47$, $p < 0.0001$; IL, ****$F_{(1,12)} = 52.13$, $p < 0.0001$; NAc, $F_{(1,12)} = 2.373$, $p = 0.1494$; LSN, ****$F_{(1,12)} = 49.99$, $p < 0.0001$; CA1, ****$F_{(1,12)} = 86.54$, $p < 0.0001$; CA2/3, ****$F_{(1,12)} = 78.93$, $p < 0.0001$; DG, ****$F_{(1,12)} = 118.5$, $p < 0.0001$; BLA, ****$F_{(1,12)} = 117.4$, $p < 0.0001$; LC, $F_{(1,12)} = 1.160$, $p = 0.3026$. **B-NET/syn/PSD95**: CG, ****$F_{(1,12)} = 35.73$, $p < 0.0001$; PL, ****$F_{(1,12)} = 34.23$, $p < 0.0001$; IL, **$F_{(1,12)} = 13.34$, $p = 0.0033$; NAc, ****$F_{(1,12)} = 50.71$, $p < 0.0001$; LSN, ****$F_{(1,12)} = 192.3$, $p < 0.0001$; CA1, ***$F_{(1,12)} = 30.61$, $p = 0.0001$; CA2/3, $F_{(1,12)} = 0.8168$, $p = 0.3839$; DG, ****$F_{(1,12)} = 116.7$, $p < 0.0001$; BLA, ****$F_{(1,12)} = 190.9$, $p < 0.0001$; LC, ****$F_{(1,12)} = 50.22$, $p < 0.0001$. Data of individual mice are shown as red dots in bars, which represent mean ± SEM ($n = 4$), *$p < 0.05$, **$p < 0.01$, ***$p < 0.001$, ****$p < 0.0001$ (Tukey's post hoc test).

Table 4. Summary of NET+ contacts with synaptic sites

Regions	WT-veh vs			cF1-veh vs
	WT-DES	cF1-veh	cF1-DES	cF1-DES
NET+ contacts to inhibitory synapses				
CG		−50% ****	−20% **	+25% *
PL	−30% ***	−30% ****	−15% *	+20% *
IL		−30% ***		+40% ****
LSN	−40% *	−50% **		+75% ****
CA1	−30% ****	−60% ****	−30% ****	+25% **
CA2/3	−50% ****	−50% ****	−30% ***	+25% *
DG	−30% **	−50% ****		+60% ****
BLA	−60% ****	−50% ***		+30% **
LC	+30% ****	−60% ****		+60% ****
NET+ contacts to excitatory synapses				
CG	−70% ****	−50% ***	−50% ***	
PL		−30% **		+30% ***
IL	−40% ****		−30% **	
NAc	−50% *		+50% ***	+50% ***
LSN	−40% ***	−40% **	+50% ****	+70% ****
CA1	−40% ***	−40% ***		+40% ***
CA2/3		−30% **		
DG	−50% ***	−50% ***	+30% *	+60% ****
BLA	−60% ****	−65% ****	−60% ****	+20% *
LC	−30% *		+30% **	+40% ****

Data from Fig. 5 are tabulated as % of vehicle-treated wild-type (WT-veh) or vehicle-treated cF1ko mouse brains (cF1-veh) versus DES-treated WT (WT-DES) or cF1ko (cF1-DES). Plus (+) and minus (−) signs denote relative increase or decrease, respectively; regions with less than 5% or nonsignificant changes are blank. See Fig. 5 for abbreviations and statistics; *$p < 0.05$, **$p < 0.01$, ***$p < 0.001$, ****$p < 0.0001$.

to inhibitory and excitatory synapses in NAc of WT mice. In cF1ko mice, several regions including mPFC (CG, PL, IL), LSN, hippocampus (CA1, CA2/3, DG), BLA, and LC showed strong reductions (30–60%) in the density of NET+ contacts with both inhibitory and excitatory synaptic sites (Table 4). The reductions in NET+ contacts with inhibitory synapses in cF1ko brains were completely or partially reversed by DES treatment. At excitatory synapses, DES reversed or increased NET+ contacts only in PL, NAc, LSN, CA1, DG, and weakly in BLA. On the other hand, in WT mice, DES reduced by 30–60% the density of inhibitory contacts in mPFC (PL), hippocampus (CA1, CA2/3, and DG), LSN, and BLA (Table 4). Excitatory contacts in DES-treated WT brains were strongly reduced by 40–70% in some of the same regions including mPFC (CG and IL), hippocampal CA1 and DG, NAc, LSN, and BLA. In the LC, cF1ko mice showed a 60% reduction in inhibitory sites with no change in excitatory sites, and DES restored inhibitory sites and increased excitatory sites, while in WT mice, DES increased inhibitory sites and reduced excitatory sites. These results indicate a strong effect of altered 5-HT activity in the cF1ko mice on the synaptic organization of the NE system with an overall reduction in NE synaptic input throughout the brain. Importantly DES treatment largely reversed this deficiency in cF1ko mice, more effectively at inhibitory sites.

We also quantified NET+ synaptic triads, in which NET +/synaptophysin staining is proximal to gephyrin+ inhibitory synapse (either the pre- or postsynaptic side) or to a PSD95+ excitatory synapse (Figs. 6, 7). Figure 6A presents a reconstructed image (see Materials and Methods) of synaptophysin within and outside of a NET+ axon outline (Syn in or Syn out) in the CG of WT mice. A pre-synaptic contact with either inhibitory (Syn in/gephyrin) or excitatory (Syn in/PSD95) synapse is shown, where Syn out is located within 0.6 µm of gephyrin or PSD95 and NET+ Syn in. In cF1ko mice, inhibitory triads were greatly reduced (30–50%) in NAc, DG (pre-synaptic only), and BLA and slightly

(5–10%) reduced in CA1, CA2/3, and LC (Table 5). DES treatment in cF1ko mice completely reversed reductions in inhibitory triads in all affected regions except CA1 and LC. Oppositely in WT mice DES significantly decreased pre-synaptic inhibitory triads in CA1 and LC and postsynaptic triads in NAc, DG, and LC (Fig. 6B,C). For excitatory triads (Fig. 7A) in cF1ko versus WT mice, a reduction in pre-synaptic triads (30%, Table 5) was seen in CA2/3 and NAc, with a slight reduction in LC (Fig. 7B). DES treatment restored these changes and increased triads in DG and DR. For postsynaptic excitatory triads, in cF1ko mice moderate reductions (10–20%) were seen in mPFC (PL, IL) and NAc (Fig. 7C, Table 5). DES treatment reversed these changes in cF1ko mice. Oppositely, in WT mice, DES treatment reduced excitatory triads in several areas including NAc, CA1, and LC (pre-synaptic) and PL, IL, NAc, and LC (postsynaptic). Thus, cF1ko mice show widespread reductions in NE synaptic triads, with the most striking changes seen in hippocampal DG and BLA (inhibitory triads) and CA2/3, IL, and NAc (excitatory triads). DES treatment also had opposite actions to reverse reductions seen in cF1ko mice, while in WT mice, DES-induced reductions were comparable to those seen in cF1ko mice.

Discussion

DES reverses behavioral deficits in cF1ko mice

We have used cF1ko mice as a model of SSRI-resistant anxiety and depression, based on the overexpression of 5-HT1A autoreceptors (Vahid-Ansari et al., 2017), which is also seen in SSRI-resistant MDD subjects (Hesselgrave and Parsey, 2013). We hypothesized that DES, which requires NE for its antidepressant actions (Cryan et al., 2001), would ameliorate behavior in cF1ko mice (Vahid-Ansari et al., 2017). In contrast to fluoxetine, chronic DES treatment improved anxiety and depression phenotypes suggesting that by enhancing NE neurotransmission (Danysz et al., 1986), DES mediates behavioral improvement despite reduced 5-HT activity in cF1ko mice. Consistent with this, in mice lacking serotonin transporter (SERT) that do not respond to fluoxetine, DES antidepressant response is unaffected or even enhanced (Mitchell et al., 2015, 2017).

Interestingly, mice with gene knock-in of the human BDNF Val66Met polymorphisic variant have reduced levels of BDNF, which was associated with increased sensitivity to stress-induced depression-related behaviors. Like cF1ko mice, while fluoxetine was ineffective, chronic DES reversed depression-like behaviors in BDNF-Met mice (Chen et al., 2006; Yu et al., 2012). Fluoxetine and DES (or imipramine) both signal in part through induction of BDNF, particularly in the hippocampus and forebrain, to mediate antidepressant responses in neurogenesis and behavior (Monteggia et al., 2004; Sairanen et al., 2005; Jin et al., 2017). However, these experiments suggest a lesser dependence of DES on BDNF (Chen et al., 2006; Yu et al., 2012). Thus, DES may enhance behavior through direct actions of NE at target areas such as mPFC, BLA, or others (McCall et al., 2017; Uematsu et al., 2017; Giustino and Maren, 2018; Poe et al., 2020). DES may also indirectly elicit NE-induced activation of dopaminergic neurons of the ventral tegmental area (VTA) (Isingrini et al., 2016; Zhang et al., 2019). In contrast, fluoxetine appears to drive 5-HT-induced behavioral improvement in part via induction of BDNF and hippocampal neurogenesis (Homberg et al., 2014; Samuels et al., 2015; Kraus et al., 2017).

While human depression is almost twofold more prevalent in women (Albert, 2015), a limitation of this model is that we do not see a strong sex difference comparing cF1ko to WT mice (Vahid-
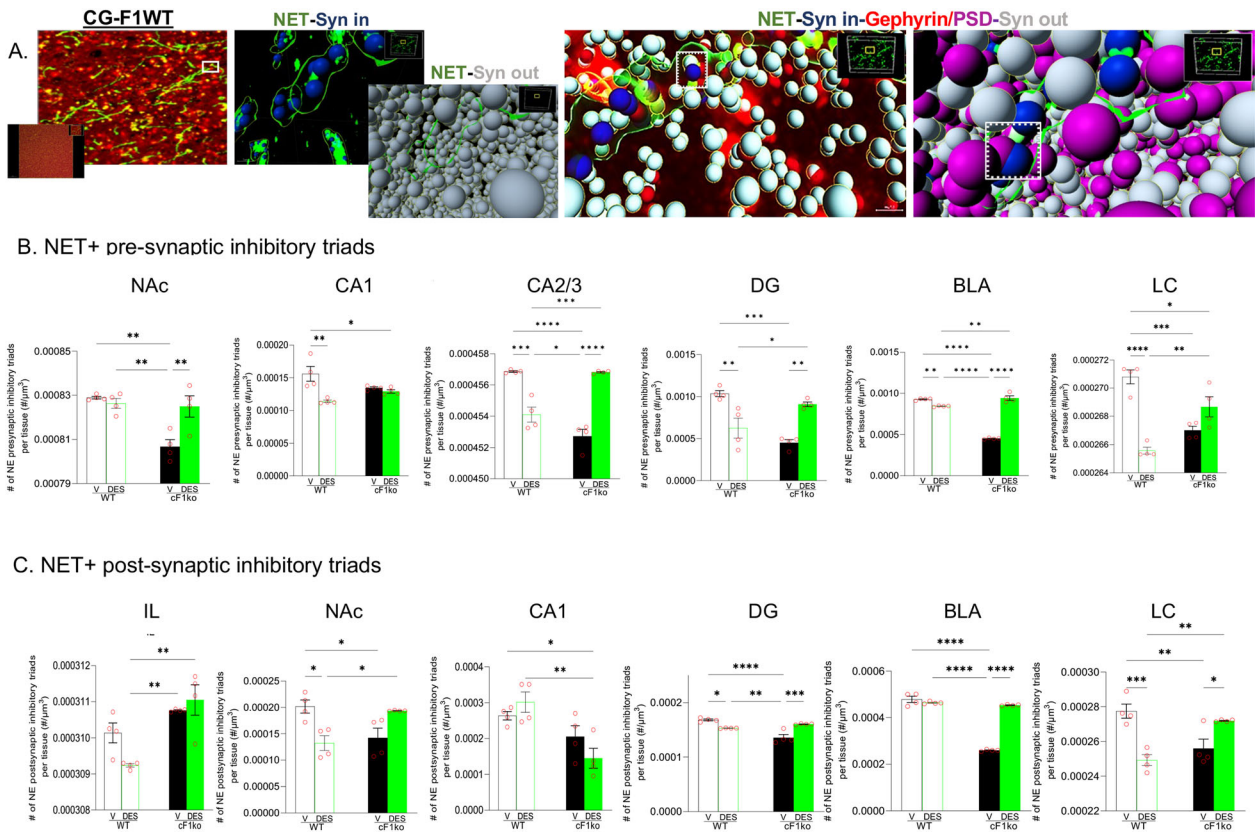
Figure 6. Chronic DES selectively re-establishes inhibitory synaptic NET+ triadic contacts in cF1ko mice. WT or cF1ko mice were treated with DES or vehicle (V) for 5 weeks and then sacrificed for immunostaining. Sections were stained for NET, pre-synaptic marker synaptophysin, and postsynaptic marker gephyrin to visualize NE inhibitory triads. *A*, Shown are representative of inhibitory triad formation of stained CG-F1WT reconstructed in IMARIS. Synaptophysin is either within (Syn in, blue) or outside (Syn out, gray) of a NET+ axon (green trace); Syn in proximal (0.6 µm) to gephyrin or PSD95 were counted as pre-synaptic triads (***B***); Syn proximal to NET+ axon and gephyrin or PSD95 were counted as postsynaptic triads (***C***). *B*, Significant reductions in pre-synaptic inhibitory NE triads in cF1ko. Syn in+ boutons within NET+ fibers located within a distance of 0.6 µm of inhibitory (gephyrin+ puncta) were quantified and normalized to tissue volume. Reductions seen in cF1ko mice were reversed by DES treatment. *C*, Significant reductions in postsynaptic inhibitory NE triads in cF1ko. Syn out/NET+ boutons within 0.6 µm of inhibitory (NET-/synaptophysin+ boutons within 0.6 µm of gephyrin+ puncta) synapses were quantified and normalized to tissue volume. Data were analyzed by region using two-way ANOVA: **B = Pre**: **NAc**, $F_{(1,12)} = 11.00$, $p = $**0.0062**; **CA1**, $F_{(1,12)} = 9.605$, **$p = 0.0092$**; **CA2/3**, $F_{(1,12)} = 114.2$, ****$p < 0.0001$; **DG**, $F_{(1,12)} = 43.69$, ****$p < 0.0001$; **BLA**, $F_{(1,12)} = 404.7$, ****$p < 0.0001$; **LC**, $F_{(1,12)} = 53.04$, ****$p < 0.0001$. **C = Post**: **IL**, $F_{(1,12)} = 5.542$, *$p = 0.0364$; **NAc**, $F_{(1,12)} = 21.21$, ***$p = 0.0006$; **CA1**, $F_{(1,12)} = 3.651$, $p = 0.0802$; **DG**, $F_{(1,12)} = 43.67$, ****$p < 0.0001$; **BLA**, $F_{(1,12)} = 237.0$, ****$p < 0.0001$; **LC**, $F_{(1,12)} = 35.09$, ****$p < 0.0001$. Data points are shown as red dots; the bars represent mean ± SEM ($n = 4$), *$p < 0.05$, **$p < 0.01$, ***$p < 0.001$, ****$p < 0.0001$ (Tukey's post hoc test).

Ansari et al., 2017). In contrast, mice with conditional knockout of MeCP2 in 5-HT neurons showed sex differences in behavioral tests compared to WT mice (Philippe et al., 2018), as did Deaf1 knockout mice (Luckhart et al., 2016). It may be that the less pronounced behavioral phenotypes in these lines reveal the presence of sex differences.

Although the generalizability of the cF1ko model to human depression may be limited, these results suggest that targeting NE may be a viable approach to the treatment of people with SSRI-resistant depression. In a comprehensive meta-analysis of trials including 21 antidepressants, the tricyclic amitriptyline (same class as DES) was the most effective, although it had higher dropout rates than those in SSRI antidepressants (Cipriani et al., 2018). This efficacy may reflect in part activity in SSRI-resistant patients. Other antidepressants that target NE may also be considered including SNRIs (venlafaxine, duloxetine), bupropion, or alpha2-adrenergic antagonist mirtazapine.

Opposite actions of DES in WT and cF1ko mice
In contrast to behavioral improvement in cF1ko mice, DES had no effect or worsened anxiety (in the EPM and NSF tests) and depression (in FST) phenotypes in WT littermate mice. In

studies using chronic DES in administered water, a trend for DES-induced increased FST immobility was seen in WT mice (Nakamoto et al., 2020) or no effect (Benham et al., 2017). On the other hand, DES in drinking water for 4 weeks reduced latency to feed in NSF (EPM and FST were not tested) (Santarelli et al., 2003). These different findings are consistent with evidence that response to chronic DES can vary by mouse strain (Yalcin et al., 2008), stress, and age (Mitchell et al., 2015).

Associated with adverse DES behaviors in WT mice, DES strongly induced FosB-labeled GABAergic cells in mPFC, while reducing them in hippocampal CA2/3, LSN, and BLA, whereas in cF1ko mice, no effect (mPFC, LSN) or opposite effect (induction in CA2/3 and BLA) was seen. This indicates that DES has very different actions in a background of normal (in WT) versus low 5-HT (in cF1ko) activity. Consistent with this, DES's antidepressant activity was enhanced in SERT−/− (low 5-HT) compared to WT mice (Mitchell et al., 2015). This paradoxical response to DES in WT mice may suggest that blocking the reuptake of both 5-HT and NE may over-activate these systems to induce anxiety (Albert et al., 2014). Oppositely, in cF1ko mice with reduced 5-HT activity, DES reverses depression and anxiety phenotypes by targeting the NE system.
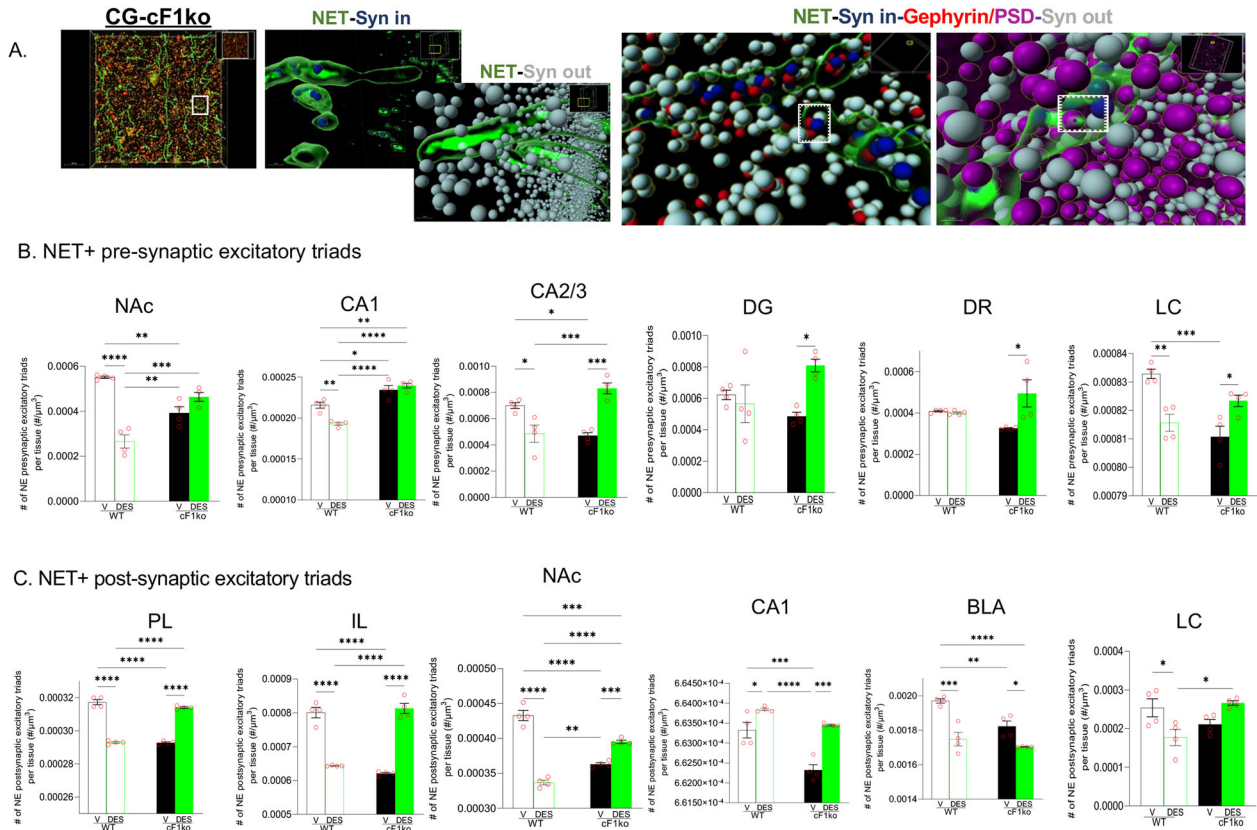
Figure 7. Chronic DES selectively re-establishes excitatory synaptic triads in cF1ko mouse. WT or cF1ko mice were treated with DES or vehicle for 5 weeks and then sacrificed for immunostaining. Sections were stained for NET, pre-synaptic synaptophysin, and postsynaptic PSD95 (NE excitatory triads). *A*, Shown are representative of excitatory triad formation of stained CG reconstructed in IMARIS. *B*, Significant reductions in pre-synaptic excitatory NE triads in cF1ko. Synaptophysin+ puncta located within NET+ fibers (Syn in) located within a distance of 0.6 μm of excitatory PSD95+ puncta were quantified and normalized to tissue volume. Reductions seen in cF1ko mice were reversed by DES treatment. *C*, Significant reductions in postsynaptic excitatory NE triads in cF1ko. Synaptophysin out/NET- boutons within 0.6 μm of excitatory PSD95+ (NET-/synaptophysin+ boutons within 0.6 μm of PSD95+ puncta) synapses were quantified and normalized to tissue volume. Data were analyzed by region using two-way ANOVA: **B = Pre**: NAc, ****$F_{(1,12)} = 62.70$, $p < 0.0001$; CA1, **$F_{(1,12)} = 14.78$, $p = 0.0023$; CA2/3, ****$F_{(1,12)} = 46.57$, $p < 0.0001$; *DG, $F_{(1,12)} = 8.191$, $p = 0.0143$; *DR, $F_{(1,12)} = 7.205$, $p = 0.0199$; ***LC, $F_{(1,12)} = 29.99$, $p = 0.0001$. **C = Post**: ****PL, $F_{(1,12)} = 649.4$, $p < 0.0001$; ****IL, $F_{(1,12)} = 258.9$, $p < 0.0001$; ****NAc, $F_{(1,12)} = 220.7$, $p < 0.0001$; CA1, *$F_{(1,12)} = 6.218$, $p = 0.0282$; BLA, $F_{(1,12)} = 3.969$, $p = 0.0696$; LC, **$F_{(1,12)} = 14.59$, $p = 0.0024$. Data points are shown as red dots; the bars represent mean ± SEM ($n = 4$), *$p < 0.05$, **$p < 0.01$, ***$p < 0.001$, ****$p < 0.0001$ (Tukey's post hoc test).

DES restores NE innervation deficits in cF1ko mice

Our previous finding that chronic fluoxetine partially restores the loss of NE innervation after stroke in the left mPFC (Zahrai et al., 2020) suggests that fluoxetine can influence NE projections. Oppositely, in cF1ko mice, NE innervation to several corticolimbic areas was reduced particularly in NE synapses in the mPFC, LSN, BLA, hippocampus, and NAc. Thus, chronic (within weeks in cF1ko mice) reduction of 5-HT activity only in adulthood is sufficient to alter NE innervation in target regions implicated in anxiety and depression phenotypes. This effect of reduced 5-HT activity on NE synapses may involve 5-HT projections to LC interneurons, leading to the dis-inhibition of NE neurons (Blier and El Mansari, 2013). Alternately, NE synapses may be modulated by 5-HT/NE cross talk in target brain regions. In rat visual cortex, both 5-HT and NE synapses have been observed by electron microscopy (Papadopoulos et al., 1987; Parnavelas and Papadopoulos, 1989). Indeed, 5-HT and NE cortical innervation overlap and modulate synapse formation (Matsukawa et al., 2003; Imai et al., 2004).

The effect of DES to largely reverse NE synaptic deficits in cF1ko mice argues that by blocking NE reuptake, DES can reverse a deficit in NE innervation. Similarly, in light-deprived mice, chronic DES treatment reversed deficits in cortical NE innervation, implicating increased NE activity in driving reinnervation (Gonzalez and Aston-Jones, 2008). The effect of DES treatment in cF1ko mice could also be mediated in part by BDNF, which has been shown to enhance cortical NE innervation in aged mice (Matsunaga et al., 2004). The actions of DES on NET+ varicosities and synapses are unlikely to involve changes in NET expression per se, since chronic DES treatment does not alter NET expression or protein levels in hippocampal or cortical regions (Erickson et al., 2011; Mitchell et al., 2013, 2017). This suggests that the neuroplasticity of monoamine systems may play a crucial role in the etiology of major depression and the actions of monoamine-targeting antidepressants. A reduction of 5-HT innervation has been observed in human depression, particularly in the orbitofrontal cortex (Rajkowska et al., 2017), but whether antidepressant treatment affects this is not known. However, drugs of abuse that target dopamine transporters affect dopamine synaptic plasticity by cadherin-dependent actions (Mills et al., 2017). Further studies are needed to address whether changes in 5-HT and NE innervation occur in human depression. The ability to quantify changes in synaptic and triadic formations within brain regions could elucidate new possibilities for targeting neuroplastic changes in monoamine pathways implicated in depression and treatment response.

Table 5. Summary of NET+ triad contacts with synaptic sites

Regions	WT-veh vs			cF1-veh vs
	WT-DES	cF1-veh	cF1-DES	cF1-DES
NET+ pre-synaptic inhibitory triads				
NAc		−5%**		+5% **
CA1	−30% **		−25% *	
CA2/3		−10% ****		+10% ****
DG	−40% **	−50% ***		+50% **
BLA	−10% **	−50% ***		+50% ****
LC	−10% ****	−10% ***	−10% *	
NET+ postsynaptic inhibitory triads				
NAc	−30% *	−30% *		
CA1			−30% *	
DG	−5% *	−10% ***		+10% ***
BLA		−50% ****		+40% ****
LC	−10% ***	−10% **		+10% *

Regions	WT-veh vs			cF1-veh vs
	WT-DES	cF1-veh	cF1-DES	cF1-DES
NET+ pre-synaptic excitatory triads				
NAc	−50%****	−30%**		
CA1	−10% **	+10% *	+10% **	
CA2/3	−30% *	−30% *		+40% ***
DG				+40% *
DR				+30% *
LC	−5%**	−5%***		+5%*
NET+ postsynaptic excitatory triads				
PL	−10% ****	−10% ****		+10% ****
IL	−15% ****	−20% ****		+20% ****
NAc	−20% ****	−20% ****	−10% ***	+5% ***
BLA	−15% ***	−10% **	−20% ****	−10% *
LC	−30% *			

Data from Figs. 6 and 7 are tabulated as % of vehicle-treated wild-type (WT-veh) or vehicle-treated cF1ko mouse brains (cF1-veh) versus DES-treated WT (WT-DES) or cF1ko (cF1-DES). Plus (+) and minus (−) signs denote relative increase or decrease, respectively; regions with less than 5% or nonsignificant changes are blank; see Figs. 6 and 7 for abbreviations and statistics; *p < 0.05, **p < 0.01, ***p < 0.001, ****p < 0.0001.

DES partly restores cellular activation changes in cF1ko mice

Consistent with the inhibitory action of overexpressed 5-HT1A autoreceptors in cF1ko mice (Vahid-Ansari et al., 2017), reduced FosB+ cell density was seen in the DR (Fig. 2), as well as reduced density of NE axons (Fig. 3). Several brain regions with reduced NE innervation in cF1ko mice also displayed reduced cellular activation, especially in lateral septum (60%), hippocampus CA2/3 (60%), and EC (30%), the latter consistent with impairment in the trisynaptic hippocampal circuit implicated in emotional memory (Anacker and Hen, 2017). These reductions in FosB+ cells were mainly in GABAergic cells, but also glutamatergic cells in CA2/3, and were matched with reductions in NE synapses to inhibitory (50%) and excitatory boutons (30%) in these areas (Fig. 5). Chronic DES treatment restored activity and NE innervation patterns in cF1ko mice to WT levels, particularly in CA2/3 and EC. Reduced LSN GABA activity could contribute to the depression phenotype in cF1ko mice since the deactivation of LSN somatostatin+ interneurons mediates depression-like behavior in chronically stressed mice (Li et al., 2022).

In the cF1ko mice, strong reductions in NE synapses to GABA boutons occurred in the hippocampus, including DG (50%, Table 4). Increases in hippocampal adult-born granule cells to enhance GABAergic activity are implicated in SSRI-induced stress resilience (Anacker and Hen, 2017; Anacker et al., 2018), suggesting that reduced NE innervation might promote stress sensitivity and fear generalization. Conversely, excitatory ventral hippocampus projections to the BLA drive anxiety (Felix-Ortiz et

al., 2013) and social avoidance via FosB activation (Eagle et al., 2020), implicating FosB elevation in BLA in the anxiety phenotype of cF1ko mice. In the BLA, DES reduced FosB+ GABAergic cells in WT but increased FosB+ pyramidal cells in cF1ko mice. Recent findings indicate that activation of GABA cells and inactivation of pyramidal cells in the BLA increases anxiogenic and social avoidance (Yu et al., 2022). Oppositely, DES-induced activation of BLA pyramidal cells in cF1ko mice may reduce anxiety, while its inhibition of GABA cells in WT mice may increase anxiety.

Conclusion

Our findings indicate the remarkable plasticity of the noradrenergic system and its role in behavioral response. Although the cF1ko knockout is specific to reducing the activity of adult 5-HT neurons, within weeks widespread actions on noradrenergic projections are observed, indicating a strong influence of 5-HT activity on adult NE plasticity. Altered NE innervation could contribute to the anxiety–depression phenotype and associated cellular activity changes seen in cF1ko mice. Consistent with this is the reversal within weeks of many of these changes by DES treatment. These findings suggest that in this model of low 5-HT activity associated with SSRI resistance, treatment with compounds that target other systems like the noradrenergic system is more effective in reversing anxiety–depression phenotypes.

References

Albert PR (2015) Why is depression more prevalent in women? J Psychiatry Neurosci 40:219–221.

Albert PR, Le Francois B, Millar AM (2011) Transcriptional dysregulation of 5-HT1A autoreceptors in mental illness. Mol Brain 4:21.

Albert PR, Lemonde S (2004) 5-HT1A receptors, gene repression, and depression: guilt by association. Neuroscientist 10:575–593.

Albert PR, Vahid-Ansari F, Luckhart C (2014) Serotonin-prefrontal cortical circuitry in anxiety and depression phenotypes: pivotal role of pre- and post-synaptic 5-HT1A receptor expression. Front Behav Neurosci 8:199.

Anacker C, Hen R (2017) Adult hippocampal neurogenesis and cognitive flexibility - linking memory and mood. Nat Rev Neurosci 18:335–346.

Anacker C, Luna VM, Stevens GS, Millette A, Shores R, Jimenez JC, Chen B, Hen R (2018) Hippocampal neurogenesis confers stress resilience by inhibiting the ventral dentate gyrus. Nature 559:98–102.

Artigas F, Bortolozzi A, Celada P (2018) Can we increase speed and efficacy of antidepressant treatments? Part I: general aspects and monoamine-based strategies. Eur Neuropsychopharmacol 28:445–456.

Belmer A, Klenowski PM, Patkar OL, Bartlett SE (2017) Mapping the connectivity of serotonin transporter immunoreactive axons to excitatory and inhibitory neurochemical synapses in the mouse limbic brain. Brain Struct Funct 222:1297–1314.

Benham RS, Hewage NB, Suckow RF, Engin E, Rudolph U (2017) Prodepressant- and anxiogenic-like effects of serotonin-selective, but not noradrenaline-selective, antidepressant agents in mice lacking alpha2-containing GABAA receptors. Behav Brain Res 332:172–179.

Blier P, El Mansari M (2013) Serotonin and beyond: therapeutics for major depression. Philos Trans R Soc Lond B Biol Sci 368:20120536.

Boldrini M, Underwood MD, Mann JJ, Arango V (2008) Serotonin-1A autoreceptor binding in the dorsal raphe nucleus of depressed suicides. J Psychiatr Res 42:433–442.

Booij L, Tremblay RE, Szyf M, Benkelfat C (2015) Genetic and early environmental influences on the serotonin system: consequences for brain development and risk for psychopathology. J Psychiatry Neurosci 40:5–18.

Chen ZY, et al. (2006) Genetic variant BDNF (Val66Met) polymorphism alters anxiety-related behavior. Science 314:140–143.

Cipriani A, et al. (2018) Comparative efficacy and acceptability of 21 antidepressant drugs for the acute treatment of adults with major depressive disorder: a systematic review and network meta-analysis. Lancet 391:1357–1366.

Cryan JF, Dalvi A, Jin SH, Hirsch BR, Lucki I, Thomas SA (2001) Use of dopamine-β-hydroxylase-deficient mice to determine the role of norepinephrine in the mechanism of action of antidepressant drugs. J Pharmacol Exp Ther 298:651–657. URL: https://www.ncbi.nlm.nih.gov/pubmed/11454927.

Danysz W, Kostowski W, Kozak W, Hauptmann M (1986) On the role of noradrenergic neurotransmission in the action of desipramine and amitriptyline in animal models of depression. Pol J Pharmacol Pharm 38:285–298. URL: https://www.ncbi.nlm.nih.gov/pubmed/3022258.

Donaldson ZR, et al. (2016) The functional serotonin 1a receptor promoter polymorphism, rs6295, is associated with psychiatric illness and differences in transcription. Transl Psychiatry 6:e746.

Dziedzicka-Wasylewska M, Faron-Górecka A, Kuśmider M, Drozdowska E, Rogóz Z, Siwanowicz J, Caron MG, Bönisch H (2006) Effect of antidepressant drugs in mice lacking the norepinephrine transporter. Neuropsychopharmacology 31:2424–2432.

Eagle AL, et al. (2020) Circuit-specific hippocampal ΔFosB underlies resilience to stress-induced social avoidance. Nat. Commun. 11:4484.

Erickson SL, Gandhi AR, Asafu-Adjei JK, Sampson AR, Miner L, Blakely RD, Sesack SR (2011) Chronic desipramine treatment alters tyrosine hydroxylase but not norepinephrine transporter immunoreactivity in norepinephrine axons in the rat prefrontal cortex. Int J Neuropsychopharmacol 14:1219–1232.

Felix-Ortiz AC, Beyeler A, Seo C, Leppla CA, Wildes CP, Tye KM (2013) BLA to vHPC inputs modulate anxiety-related behaviors. Neuron 79:658–664.

Fogarty MJ, Hammond LA, Kanjhan R, Bellingham MC, Noakes PG (2013) A method for the three-dimensional reconstruction of neurobiotin-filled neurons and the location of their synaptic inputs. Front Neural Circuits 7:153.

Garcia-Garcia AL, Newman-Tancredi A, Leonardo ED (2014) 5-HT(1A) receptors in mood and anxiety: recent insights into autoreceptor versus heteroreceptor function. Psychopharmacology (Berl) 231:623–636.

Giustino TF, Maren S (2018) Noradrenergic modulation of fear conditioning and extinction. Front Behav Neurosci 12:43.

Gonzalez MM, Aston-Jones G (2008) Light deprivation damages monoamine neurons and produces a depressive behavioral phenotype in rats. Proc Natl Acad Sci U S A 105:4898–4903.

Gray NA, Milak MS, Delorenzo C, Ogden RT, Huang YY, Mann JJ, Parsey RV (2013) Antidepressant treatment reduces serotonin-1A autoreceptor binding in major depressive disorder. Biol Psychiatry 74:26–31.

Hesselgrave N, Parsey RV (2013) Imaging the serotonin 1A receptor using [11C]WAY100635 in healthy controls and major depression. Philos Trans R Soc Lond B Biol Sci 368:20120004.

Homberg JR, Molteni R, Calabrese F, Riva MA (2014) The serotonin-BDNF duo: developmental implications for the vulnerability to psychopathology. Neurosci Biobehav Rev 43:35–47.

Imai H, Matsukawa M, Okado N (2004) Lamina-selective changes in the density of synapses following perturbation of monoamines and acetylcholine in the rat medial prefrontal cortex. Brain Res 1012:138–145.

Isingrini E, et al. (2016) Resilience to chronic stress is mediated by noradrenergic regulation of dopamine neurons. Nat Neurosci 19:560–563.

Jacobsen KX, Vanderluit JL, Slack RS, Albert PR (2008) HES1 regulates 5-HT1A receptor gene transcription at a functional polymorphism: essential role in developmental expression. Mol Cell Neurosci 38:349–358.

Jans LA, Riedel WJ, Markus CR, Blokland A (2007) Serotonergic vulnerability and depression: assumptions, experimental evidence and implications. Mol Psychiatry 12:522–543.

Jin HJ, et al. (2017) Alleviative effects of fluoxetine on depressive-like behaviors by epigenetic regulation of BDNF gene transcription in mouse model of post-stroke depression. Sci Rep 7:14926.

Kautzky A, et al. (2017) The influence of the rs6295 gene polymorphism on serotonin-1A receptor distribution investigated with PET in patients with major depression applying machine learning. Transl Psychiatry 7:e1150.

Kennedy SH, et al. (2016) Canadian network for mood and anxiety treatments (CANMAT) 2016 clinical guidelines for the management of adults with major depressive disorder: section 3. Pharmacological treatments. Can J Psychiatry 61:540–560.

Klenowski PM, Fogarty MJ, Belmer A, Noakes PG, Bellingham MC, Bartlett SE (2015) Structural and functional characterization of dendritic arbors and GABAergic synaptic inputs on interneurons and principal cells in the rat basolateral amygdala. J Neurophysiol 114:942–957.

Kraus C, Castren E, Kasper S, Lanzenberger R (2017) Serotonin and neuroplasticity - links between molecular, functional and structural pathophysiology in depression. Neurosci Biobehav Rev 77:317–326.

Krishnan V, Nestler EJ (2008) The molecular neurobiology of depression. Nature 455:894–902.

Lemonde S, et al. (2003) Impaired repression at a 5-hydroxytryptamine 1A receptor gene polymorphism associated with major depression and suicide. J Neurosci 23:8788–8799.

Le Poul E, Boni C, Hanoun N, Laporte AM, Laaris N, Chauveau J, Hamon M, Lanfumey L (2000) Differential adaptation of brain 5-HT1A and 5-HT1B receptors and 5-HT transporter in rats treated chronically with fluoxetine. Neuropharmacology 39:110–122.

Li H, Sung HH, Lau CG (2022) Activation of somatostatin-expressing neurons in the lateral septum improves stress-induced depressive-like behaviors in mice. Pharmaceutics 14:2253.

Luckhart C, Philippe TJ, Le Francois B, Vahid-Ansari F, Geddes SD, Beique JC, Lagace DC, Daigle M, Albert PR (2016) Sex-dependent adaptive changes in serotonin-1A autoreceptor function and anxiety in Deaf1-deficient mice. Mol Brain 9:77.

Matsukawa M, Nakadate K, Ishihara I, Okado N (2003) Synaptic loss following depletion of noradrenaline and/or serotonin in the rat visual cortex: a quantitative electron microscopic study. Neuroscience 122:627–635.

Matsunaga W, Shirokawa T, Isobe K (2004) BDNF is necessary for maintenance of noradrenergic innervations in the aged rat brain. Neurobiol Aging 25:341–348.

McCall JG, Siuda ER, Bhatti DL, Lawson LA, McElligott ZA, Stuber GD, Bruchas MR (2017) Locus coeruleus to basolateral amygdala noradrenergic projections promote anxiety-like behavior. Elife 6:e18247.

Mills F, Globa AK, Liu S, Cowan CM, Mobasser M, Phillips AG, Borgland SL, Bamji SX (2017) Cadherins mediate cocaine-induced synaptic plasticity and behavioral conditioning. Nat Neurosci 20:540–549.

Mitchell NC, Bowman MA, Gould GG, Koek W, Daws LC (2017) Ontogeny of norepinephrine transporter expression and antidepressant-like response to desipramine in wild-type and serotonin transporter mutant mice. J Pharmacol Exp Ther 360:84–94.

Mitchell NC, Gould GG, Smolik CM, Koek W, Daws LC (2013) Antidepressant-like drug effects in juvenile and adolescent mice in the tail suspension test: relationship with hippocampal serotonin and norepinephrine transporter expression and function. Front Pharmacol 4:131.

Mitchell NC, Koek W, Daws LC (2015) Antidepressant-like effects and basal immobility depend on age and serotonin transporter genotype. Genes Brain Behav 14:543–549.

Monteggia LM, Barrot M, Powell CM, Berton O, Galanis V, Gemelli T, Meuth S, Nagy A, Greene RW, Nestler EJ (2004) Essential role of brain-derived neurotrophic factor in adult hippocampal function. Proc Natl Acad Sci U S A 101:10827–10832.

Nakamoto C, Kawamura M, Nakatsukasa E, Natsume R, Takao K, Watanabe M, Abe M, Takeuchi T, Sakimura K (2020) Glud1 knockout mice with a pure C57BL/6N background show impaired fear memory, social interaction, and enhanced depressive-like behavior. PLoS One 15:e0229288.

Nestler EJ (2015) Fosb: a transcriptional regulator of stress and antidepressant responses. Eur J Pharmacol 753:66–72.

Papadopoulos GC, Parnavelas JG, Buijs R (1987) Monoaminergic fibers form conventional synapses in the cerebral cortex. Neurosci Lett 76:275–279.

Parnavelas JG, Papadopoulos GC (1989) The monoaminergic innervation of the cerebral cortex is not diffuse and nonspecific. Trends Neurosci 12:315–319.

Parsey RV, et al. (2010) Higher serotonin 1A binding in a second major depression cohort: modeling and reference region considerations. Biol Psychiatry 68:170–178.

Parsey RV, Olvet DM, Oquendo MA, Huang YY, Ogden RT, Mann JJ (2006) Higher 5-HT1A receptor binding potential during a major depressive episode predicts poor treatment response: preliminary data from a naturalistic study. Neuropsychopharmacology 31:1745–1749.

Paxinos G, Franklin KBJ (2001) The mouse brain in stereotaxic coordinates, Ed 2nd. San Diego, CA: Academic Press.

Philippe TJ, et al. (2018) Loss of MeCP2 in adult 5-HT neurons induces 5-HT1A autoreceptors, with opposite sex-dependent anxiety and depression phenotypes. Sci Rep 8:5788.

Poe GR, et al. (2020) Locus coeruleus: a new look at the blue spot. Nat Rev Neurosci 21:644–659.

Rainer Q, Nguyen HT, Quesseveur G, Gardier AM, David DJ, Guiard BP (2012) Functional status of somatodendritic serotonin 1A autoreceptor after long-term treatment with fluoxetine in a mouse model of anxiety/depression based on repeated corticosterone administration. Mol Pharmacol 81:106–112.

Rajkowska G, et al. (2017) Length of axons expressing the serotonin transporter in orbitofrontal cortex is lower with age in depression. Neuroscience 359:30–39.

Riad M, Kobert A, Descarries L, Boye S, Rompre PP, Lacaille JC (2017) Chronic fluoxetine rescues changes in plasma membrane density of 5-HT1A autoreceptors and serotonin transporters in the olfactory bulbectomy rodent model of depression. Neuroscience 356:78–88.

Riad M, Zimmer L, Rbah L, Watkins KC, Hamon M, Descarries L (2004) Acute treatment with the antidepressant fluoxetine internalizes 5-HT1A autoreceptors and reduces the in vivo binding of the PET radioligand [18F]MPPF in the nucleus raphe dorsalis of rat. J Neurosci 24:5420–5426.

Richardson-Jones JW, et al. (2010) 5-HT(1A) autoreceptor levels determine vulnerability to stress and response to antidepressants. Neuron 65:40–52.

Rush AJ, Warden D, Wisniewski SR, Fava M, Trivedi MH, Gaynes BN, Nierenberg AA (2009) STAR*D: revising conventional wisdom. CNS Drugs 23:627–647.

Sairanen M, Lucas G, Ernfors P, Castren M, Castren E (2005) Brain-derived neurotrophic factor and antidepressant drugs have different but coordinated effects on neuronal turnover, proliferation, and survival in the adult dentate gyrus. J Neurosci 25:1089–1094.

Samuels BA, et al. (2015) 5-HT1A receptors on mature dentate gyrus granule cells are critical for the antidepressant response. Nat Neurosci 18:1606–1616.

Santarelli L, et al. (2003) Requirement of hippocampal neurogenesis for the behavioral effects of antidepressants. Science 301:805–809.

Schatzle P, Wuttke R, Ziegler U, Sonderegger P (2012) Automated quantification of synapses by fluorescence microscopy. J Neurosci Methods 204:144–149.

Stockmeier CA, Shapiro LA, Dilley GE, Kolli TN, Friedman L, Rajkowska G (1998) Increase in serotonin-1A autoreceptors in the midbrain of suicide victims with major depression-postmortem evidence for decreased serotonin activity. J Neurosci 18:7394–7401.

Tremblay P, Blier P (2006) Catecholaminergic strategies for the treatment of major depression. Curr Drug Targets 7:149–158.

Trivedi MH, et al. (2006) Evaluation of outcomes with citalopram for depression using measurement-based care in STAR*D: implications for clinical practice. Am J Psychiatry 163:28–40.

Uematsu A, Tan BZ, Ycu EA, Cuevas JS, Koivumaa J, Junyent F, Kremer EJ, Witten IB, Deisseroth K, Johansen JP (2017) Modular organization of the brainstem noradrenaline system coordinates opposing learning states. Nat Neurosci 20:1602–1611.

Vahid-Ansari F, Daigle M, Manzini MC, Tanaka KF, Hen R, Geddes SD, Beique JC, James J, Merali Z, Albert PR (2017) Abrogated freud-1/Cc2d1a repression of 5-HT1A autoreceptors induces fluoxetine-resistant anxiety/depression-like behavior. J Neurosci 37:11967–11978.

Vahid-Ansari F, Zhang M, Zahrai A, Albert PR (2019) Overcoming resistance to selective serotonin reuptake inhibitors: targeting serotonin, serotonin-1A receptors and adult neuroplasticity. Front Neurosci 13:404.

Vialou V, Thibault M, Kaska S, Cooper S, Gajewski P, Eagle A, Mazei-Robison M, Nestler EJ, Robison AJ (2015) Differential induction of FosB isoforms throughout the brain by fluoxetine and chronic stress. Neuropharmacology 99:28–37.

Wagner-Altendorf TA, Fischer B, Roeper J (2019) Axonal projection-specific differences in somatodendritic α2 autoreceptor function in locus coeruleus neurons. Eur J Neurosci 50:3772–3785.

Wang G, Smith SJ (2012) Sub-diffraction limit localization of proteins in volumetric space using Bayesian restoration of fluorescence images from ultrathin specimens. PLoS Comput Biol 8:e1002671.

Warner-Schmidt J (2013) Treating the brain deep down: short-circuiting depression. Nat Med 19:680–681.

WHO (2017) Depression and other common mental disorders: global health estimates. Geneva, Switzerland: World Health Organization.

Yalcin I, Belzung C, Surget A (2008) Mouse strain differences in the unpredictable chronic mild stress: a four-antidepressant survey. Behav Brain Res 193:140–143.

Yu XD, et al. (2022) Distinct serotonergic pathways to the amygdala underlie separate behavioral features of anxiety. Nat Neurosci 25:1651–1663.

Yu H, Wang DD, Wang Y, Liu T, Lee FS, Chen ZY (2012) Variant brain-derived neurotrophic factor Val66Met polymorphism alters vulnerability to stress and response to antidepressants. J Neurosci 32:4092–4101.

Zahrai A, Vahid-Ansari F, Daigle M, Albert PR (2020) Fluoxetine-induced recovery of serotonin and norepinephrine projections in a mouse model of post-stroke depression. Transl Psychiatry 10:334.

Zhang H, et al. (2019) α(1)- and β(3)-adrenergic receptor-mediated mesolimbic homeostatic plasticity confers resilience to social stress in susceptible mice. Biol Psychiatry 85:226–236.